*Tutor*

Prof. Feliu Maseras Cuní

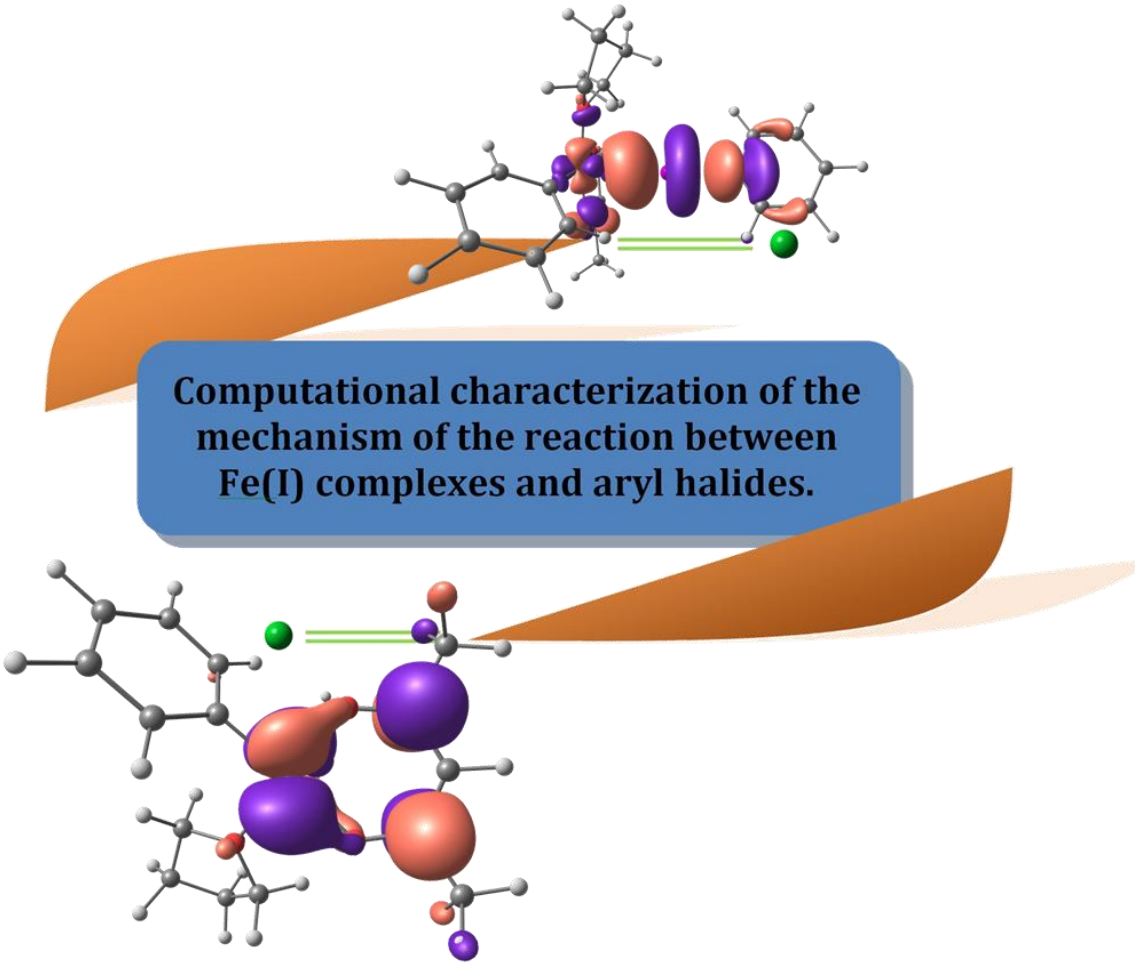


**Master in Synthesis, Catalysis and Molecular Design**
**Master Thesis**

**Lluís Artús Suàrez**
**June 2016**

ICIQ Institut Català d'Investigació Química

UNIVERSITAT ROVIRA i VIRGILI

*If I have seen further, it is by*
*standing on the shoulders of giants.*

Isaac Newton

I want to thank ICIQ and more concretely to Feliu Maseras, for giving me the opportunity of working on a first class environment with great equipment, companions and pure knowledge. Thanks to you all for not minding to spend hours in helping me through my bad and good moments. Funes deserves a special mention for his invaluable advices. And finally thanks to my entire group of companions in the master courses, my family and she.

# Contents

# ABSTRACT

This work reports a computational study through density functional theory (DFT) calculations of the mechanism of the reaction between $[Fe(acac)(THF)(Ph)]^-$ and different halobenzenes (iodo-, bromo- and chloro-) resulting in phenyl radical and halide. The key step, controlling the overall reaction rate, is the single electron transfer (SET) from the starting complex to the halobenzene. We have been able to characterize, through a broken symmetry approach, the transition state of this step for each of the studied systems. The reaction rate increases in the order chloro- < bromo- < iodo-. The leading features of the mechanism are studied through structural analysis of intermediates and transition states as well as analysis of natural and natural spin orbitals. Acetylacetonate is shown to be a non-innocent ligand, participating directly in the chlorobenzene reaction, and indirectly in the reaction with iodobenzene and bromobenzene.

# 1. INTRODUCTION

## 1.1. SINGLE ELECTRON TRANSFER (SET) IN FIRST ROW TRANSITION METALS CHEMISTRY

The chemistry of transition metal complexes has been so far dominated by two-electron processes.[1–3] Processes like oxidative addition, reductive elimination, olefin metathesis, transmetalation, which are dominant in transition metal chemistry are based on the transfer of two-electron packages from or to the metal centre. These two-electron steps are key in the most successful examples of transition metal catalysis, such as hydrogenation, olefin metathesis and cross-coupling.[4–6]

Two-electron transfer is however not the only possible reaction pattern for transition metal complexes. It has been long known that transition metal complexes may also operate in single electron transfer (SET) processes. This has been recognized in a number of reviews.[7,8] Figure 1.1 is a modified version from a scheme in one of them. In general, the activity of transition metal compounds towards organic substrates may change depending on their electronic properties and the charge of the substrate. One of the highlighted three general reaction pathways is precisely the two-electron transfer (path A). The oxidation state of the metal increases by two and the result of this process is the formation of an organometallic species with a stable metal-carbon bond. The other two reported paths, B and C, involve SET, with increase by one for the formal oxidation state in the metal. The synthetic methodology for paramagnetic organometallic complexes is not nearly as advanced as that for diamagnetic complexes, mainly of the second and third row. This may be due in part to the perception that second-row metals are more important catalytically.

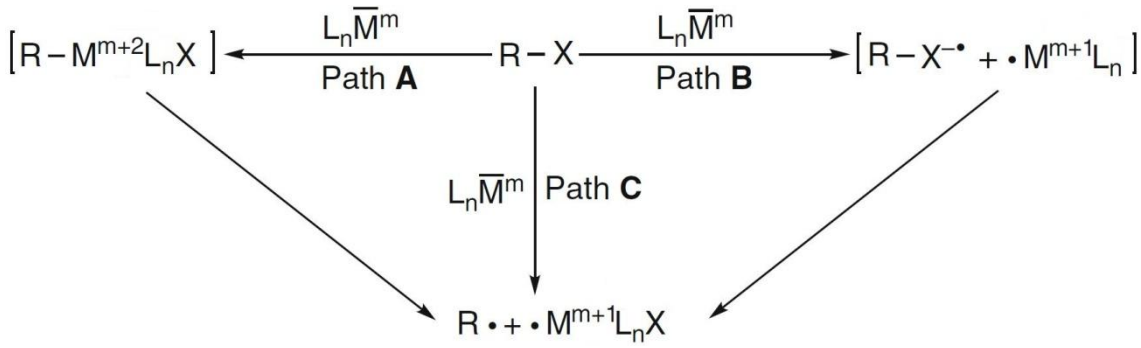


Figure 1.1. Some metal-mediated activation of organic molecules.[7]

The stability of several adjacent oxidation states effectively introduces competing SET steps to reactions based on two-electron reductive elimination or oxidative addition processes, typical of the familiar catalytic cycles based on $d^8$ and $d^{10}$ complexes of palladium[8] or $d^4$ and $d^6$ ruthenium species.[5] The potential of a metal or complexes thereof for SET can be derived very roughly by assessing its first ionization potential or its electron affinity. In general 3d metals display a lower first ionization potential than 4d or 5d metals. Consequently, low-valent metal complexes are more active in donating single electrons to organic substrates than high-valent metal complexes. The same holds in general for 3d metals in comparison with 4d or 5d metals. Thus single electron donation competes successfully with two electron oxidative additions in 3d metal complexes but less in 4d and 5d metal complexes. It must be emphasized that ligands profoundly influence the character of active metal centres so that the rationalization and comparison of experimental results must be performed at this stage with great care.

Using first-row metal starting materials in a lower oxidation state is often advantageous in order to prevent unwanted reduction during salt metathesis reactions. It can also help avoid other potential pitfalls such as “ate” complex formation or undesired metal-ligand stoichiometry. Once formed, SET oxidation of a $ML_n$ complex is useful in the synthesis of $ML_nX$ species (X = halide, OTf, etc.).[9] Such halide complexes might be synthetic targets in their own right or may serve as useful precursors for subsequent salt metathesis reactions. This stepwise strategy facilitates the construction of target molecules with distinct ancillary and reactive ligands, an important requirement in the preparation of well-defined catalysts generally, as well as in the independent synthesis of intermediates believed to participate in a proposed catalytic cycle. Alternatively, SET oxidation reactions performed using weakly

coordinating anions permit the generation of $[ML_n]^+$ cations from neutral $ML_n$ complexes. These cationic species may be amenable to the formation of metal-ligand multiple bonds via intermolecular[10,11] or intramolecular α-H abstraction reactions.[12,13] The preparation of active, well-defined, single-component catalysts by a SET oxidation process[14,15] is particularly useful for studying paramagnetic polymerization systems, where the nature of the catalytically active species generated in situ with excess alkylaluminum cocatalysts is often debatable. Some of the most exciting new paramagnetic organometallic chemistry is being conducted on iron complexes, with relevance for a range of applications, including ethylene, styrene, and acrylonitrile polymerization, hydrogenation and hydrosilation, cross-coupling reactions, reversible β-H elimination, and $N_2$ activation. The preparation of well-defined, paramagnetic Fe complexes should help to illuminate connections between these various applications, as well as delineate the role of different possible electronic configurations in these reactions.

A number of complexes can produce oxidative radical generation. High-valent oxo-complexes, either in situ-generated or isolated, interact most often with electron-rich π-systems **1** or suitable C-H bonds with low bond dissociation energy (BDE) in substrates **3** (Figure 1.2.). These reactions can occur concerted through transition states **1A** or **3A** resulting into epoxides **2** or alcohols **4**. On the other hand, a number of epoxidation reactions, such as the Jacobsen-Katsuki epoxidation, are known to proceed by a stepwise pathway via transition state**1B** to radical intermediate **1C**.[16] Similarly, oxidation of hydrocarbons to **4** may proceed by a hydrogen abstraction/$S_{RN}2$ path way via **3B** and **3C**. This mechanism is often discussed in enzyme-catalyzed oxidations, such as those induced by cytochrome P450.[17]

Other higher oxidation states metal compounds, such as complexes or simple salts of manganese(III), iron(III), copper(II) and the 2n row transition metal silver (I) act as SET oxidants for functional groups, electron-rich π-systems **5**, or anions $\mathbf{5}^-$ derived thereof (Figure 1.3.). Initially radical cations **5A** and subsequently radicals **5B** are generated. Anionic species $\mathbf{5}^-$ react mostly by transmetalation to transient metal enolate **5C** which homolyzes to radical **5B**. Free radical reactivity is often observed and the reduced form of the oxidant does not participate in the further course.

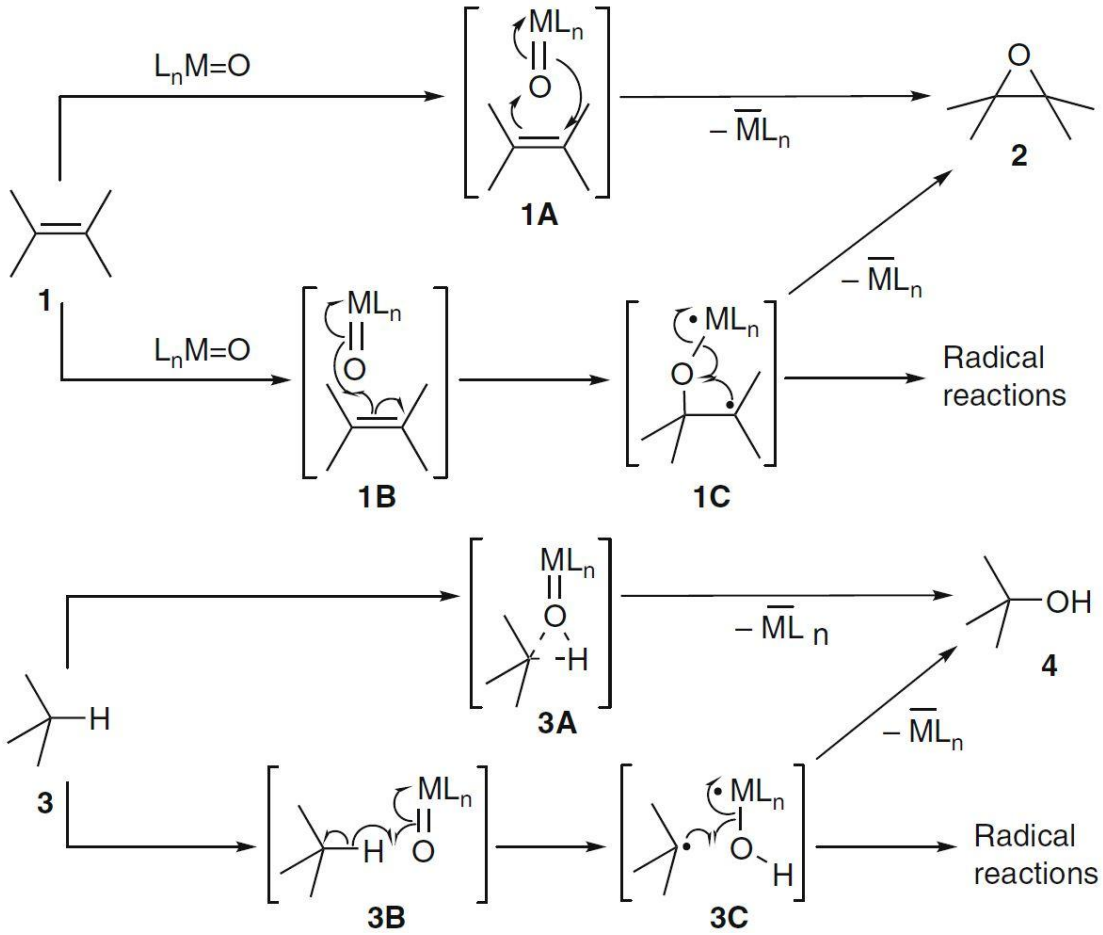


Figure 1.2. Examples of radical epoxidation and hidroxylation by metal oxo complexes.[7]

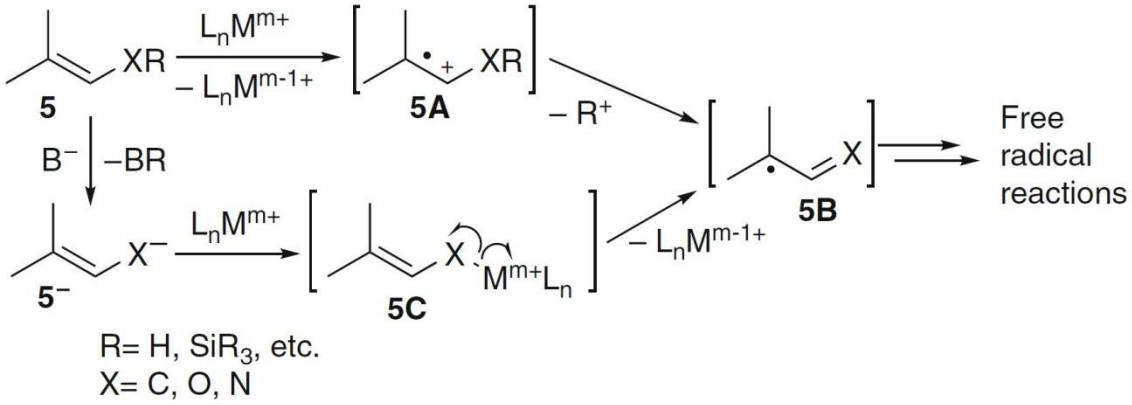


Figure 1.3. Oxidative radical generation by high-valent transition metal salts.[7]

Alternatively, other complexes are involved in reductive radical generation. Organic substrates **6** can interact in several ways with low oxidation state transition metal compounds triggering overall electroneutral or catalytic or reductive transformations dependent on the reduction capacity of the metal (Figure 1.4.). Low-valent metal complexes that are able to undergo two-electron oxidations react with halides or sulfonates **6** to organometallic intermediates **7**. Its formation can occur by an $S_N2$ process (back side attack) at carbon via **6A** manifesting itself by inversion of configuration with chiral substrates.[21] For the majority of substrates with sp- or $sp^2$-carbon-element bonds the formation of **7** proceeds through oxidative addition into the carbon-element bond via **6B**.[3] Retention of configuration is observed with chiral substrates. Some organometallic compounds **7** undergo homolytic cleavage with ease to generate a radical pair **6D** initially, which can lead to freely diffusing radicals after escaping from the solvent cage.

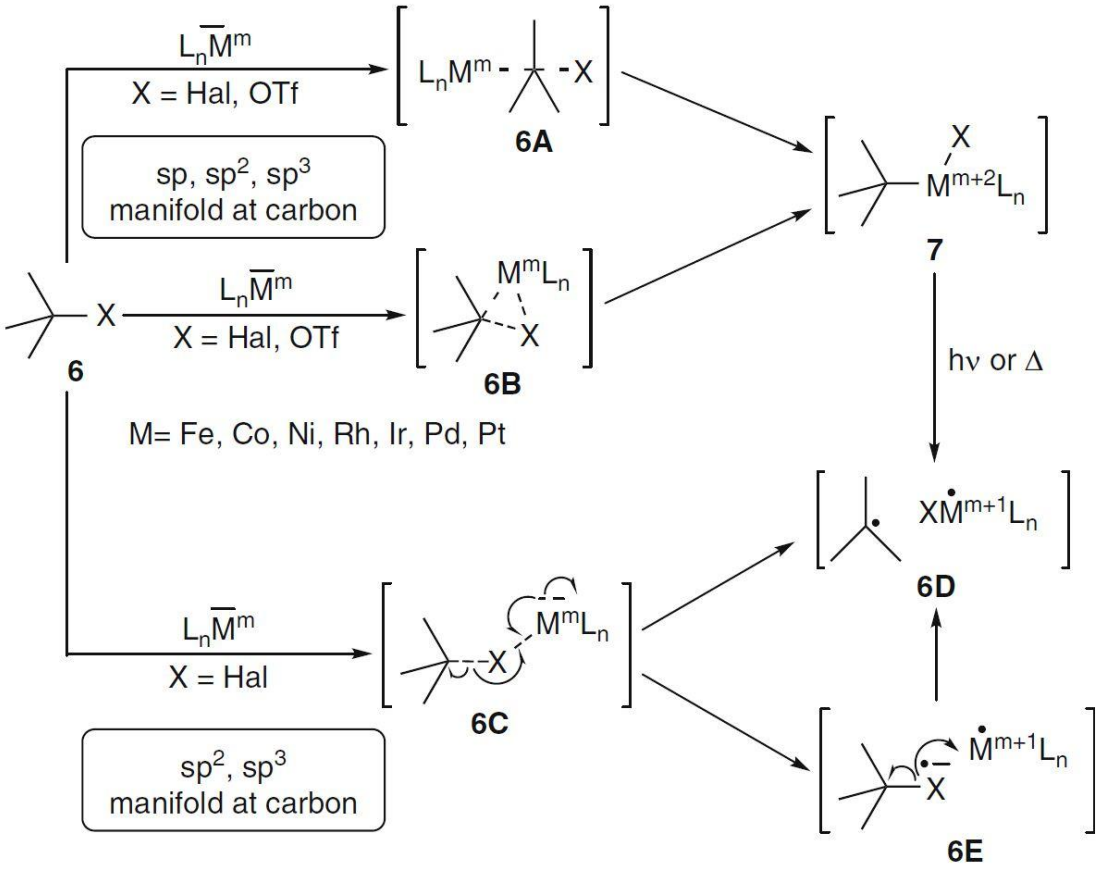


Figure 1.4. Reductive radical generation reactions of low-valent metal complexes with organic substrates.[7]

Metal salts and complexes of titanium(II,III), vanadium(III,IV), chromium(0 to II), manganese(0 to II), iron(-II to II), cobalt(0,I), nickel(0,I) and cooper(I), the second row transition metals ruthenium(II), rhodium(I), palladium(0) and silver(0) and the third row transition metal platinum(0) can donate a single electron to organic substrates. Thus, they are able to activate good electron acceptors, such as alkyl halides **6**, but also carbonyl compounds, epoxides, or peroxides (Fenton reaction) reductively. These radicals often do not couple particularly fast with the oxidized metal species and free radical reactions can be performed subsequently.

Especially for alkyl halides **6** the transfer of a single electron from the metal center is facile and occurs at the halide via transition state **6C**, which stabilizes either by direct abstraction of the halide to a carbon-metal complex radical pair **6D** or via a distinct radical anion-metal complex pair **6E**. This process was noted years ago[20] but not exploited until recently. Alkyl tosylates or triflates are not easily reduced by SET, and thus $S_N2$ and/or oxidative addition pathways are common. The generation of σ-radicals from aryl and vinyl halides has been observed, but is rarer due to the energy requirement for their generation. Normally two-electron oxidative addition prevails.

## 1.2. THE PHENYL RADICAL

Direct or indirect electrochemical reduction of aryl halides in solvents of low proton availability offers a convenient and controlled means for generation of aryl radicals. The method has been applied successfully to the addition of aryl radicals on nucleophiles triggering $S_{RN}1$ aromatic substitution reactions[21] and to reactions based on H atom abstraction by aryl radicals.[22] The indirect electrochemical reduction consists of the electrochemical generation of mediators such as aromatic anion radicals which shuttle electrons between the electrode and the aryl halide. The interest of the indirect method as compared to the direct one derives from the fact that aryl radicals are much easier to reduce than the parent aryl halides. Thus, with direct electrochemistry, in the cases where the radical generation is fast, the aryl radicals are produced close to the electrode surface and will then be reduced there before having time to trigger the chemistry of interest in the solution. In indirect electrochemistry, the generation of the aryl radical takes place in the solution, and its reduction mainly occurs by electron transfer from the reduced form of the catalyst. This again competes

with the triggering of the chemistry of interest. However, the rate of the competing side reaction corresponds at most to the diffusion limit, and one can decrease the mediator concentration to slow it down. Such strategy has been applied successfully in several instances in the case of $S_{RN}1$ aromatic substitution reactions. Some example of reactions involving aryl radicals and olefins would be the Meerwein reaction where an aryl diazonium chloride reacts with an olefin in the presence of cuprous chloride leading to either to addition of the aryl group and the chlorine atom or to substitution of one hydrogen of the double bond by the aryl group; the dehalogenation of alkyl, aryl, or vinyl halides by means of trialkyltin radicals; the photostimulated reaction of aliphatic and aromatic halides through addition to 2-naphthoxide by a $S_{RN}1$ mechanism; or the cleavage of the C–Cl bond in homogeneous media and with electrochemical devices.

## 1.3. DFT PRECEDENTS AND CHALLENGES

Marcus formulated in 1956 his theory, which settled the basis for the electron transfer description. Marcus theory originally started as an explanation to the rate at which an electron can move or jump from one chemical species in solution (called the electron donor) to another one (called the electron acceptor) in an outer sphere electron transfer reaction, and it was latter extended for inner sphere electron transfer reactions and heterogeneous electron transfer. Some of the implications of the inner sphere theory are that the distances are dependent on the charge of donor and acceptor, and that the Franck-Condon principle must be obeyed: for the electron jump to occur, the nuclei have to have a configuration which is an identical one of as well the precursor as the successor complexes. Onces that happens, the orbitals of the donnor and the acceptor can overlap (Figure 1.5).

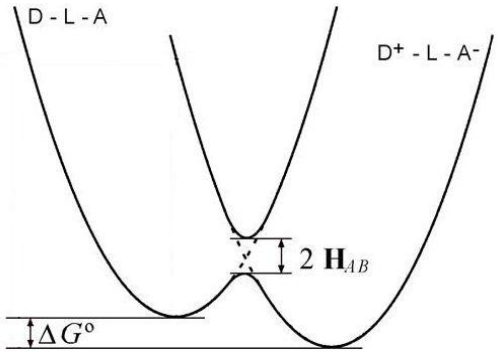


Figure 1.5. Orbital overlap ($2H_{AB}$) schematization.

This overlap suggests the formation of mixed valence compounds with poorly defined formal oxidation state which may be more appropriately viewed as being in an intermediate oxidation state.

Classic monodeterminantal wavefunctions are in principle not appropriate to describe these mixed valence compounds well, as they contain diverse electron distributions different from closed-shell. They should be just described by multiconfigurational methods such as CASSCF and related approaches. Applications of DFT functionals such as B3LYP have been in any case published.[23–25]

Some computational studies in SET reactions involving aryl halides are described in the literature,[26,27] but they stay short of studying the mechanism, much less of characterizing transition states. An interesting computational paper on a related topic is that by Hobza and co-workers discussing the sigma hole in phenyl halides and its nature (Figure 1.6.).[28]

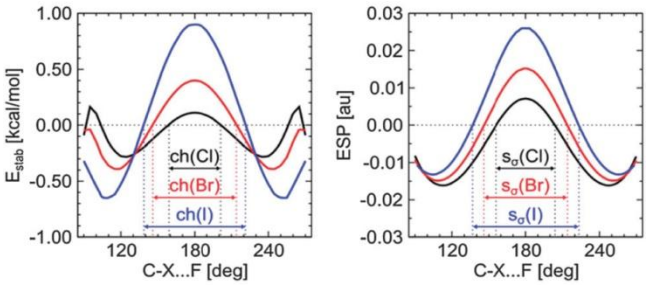


Figure 1.6. Left: The angular dependence of the stabilization energy of hydrogen fluoride with halobenzenes. The channel of attractive interaction channel is depicted. Right: The angular dependence of electrostatic potential (ESP).

## 1.4. Single Electron Transfer (SET) with Iron I complexes and aryl halides

The reactivity of iron complexes with organic halides has been mostly focused on the attempts to use iron as a replacement for palladium in cross-coupling. Iron-catalyzed cross-coupling has been achieved between with alkyl or aryl Grignard reagents and either vinyl[29,30] or aryl halides.[31] Higher reactivity is achieved in the case of vinyl halides, likely because oxidative addition is easier when there is an activating effect of from the adjacent unsaturation. This reactivity does not seem to involve organic radicals.

In this context the recent publication by Jutand and co-workers on the reactivity between $[Fe(acac)(Ph)]^-$ (acac=acetylacetonate) and iodobenzene is remarkable. The reaction results in the formation of a $Ph^\cdot$ radical and a iodide anion. The experimental mechanistic study is rather complete, involving paramagnetic NMR, magnetic measurements, EPR and cyclic voltammetries. Based on these experiments they propose the mechanism shown in Figure 1.7 for the reaction of iodobenzene.

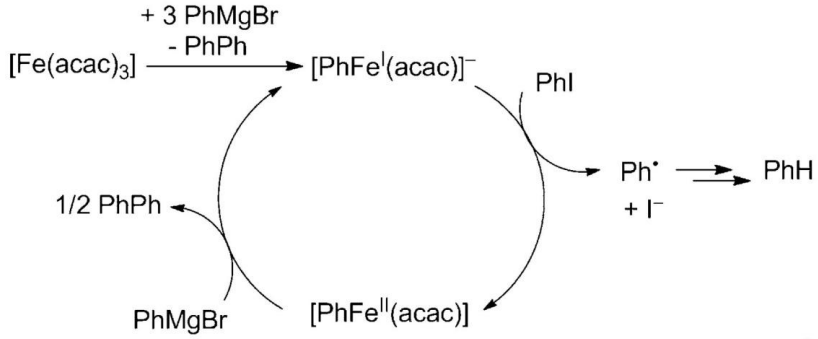


1.7. Proposed reaction mechanism for PhI reduction by PhMgBr catalysed by $[PhFe^{I}(acac)(THF)]^-$.[32] THF molecules omitted for clarity.

The thorough experimental study is complemented with limited computational studies. Calculations on the experimental publication use the PBE0 functional, without dispersion, report potential energies without free energy corrections and do not compute any transition state. The computational results reported by Jutand and co-workers are summarized in Figure 1.8.

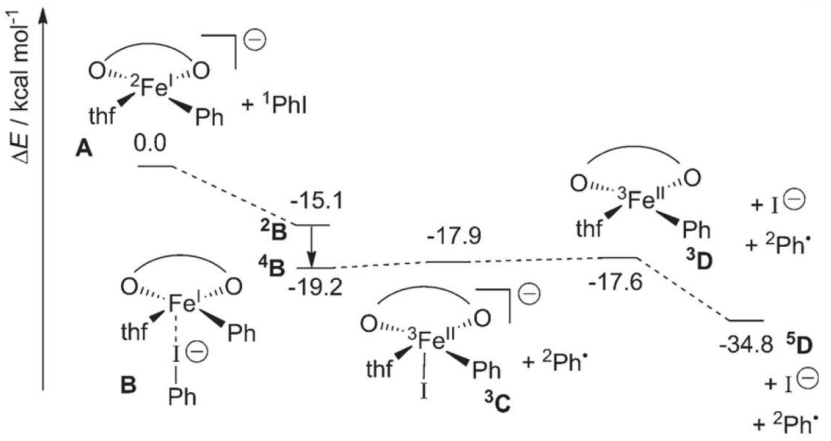


Figure 1.8. Proposed potential energy diagram for the catalytic PhI reduction pathway.[32]

The proposed pathway starts with the separate fragments A, in the doublet state, approaching to result in adduct $^2$B. Then adduct $^2$B, in doublet state, evolves somehow to adduct $^4$B, in the quartet state. This intermediate $^4$B loses a phenyl radical and a

iodine anion resulting in intermediate $^{3}$D, in the triplet state. The triplet intermediate evolves to the quintet product $^{5}$D, again by some unspecified mechanism.

The mechanism of the reaction with bromobenzene was also studied computationally in the same publication. Results are summarized in Figure 1.9.

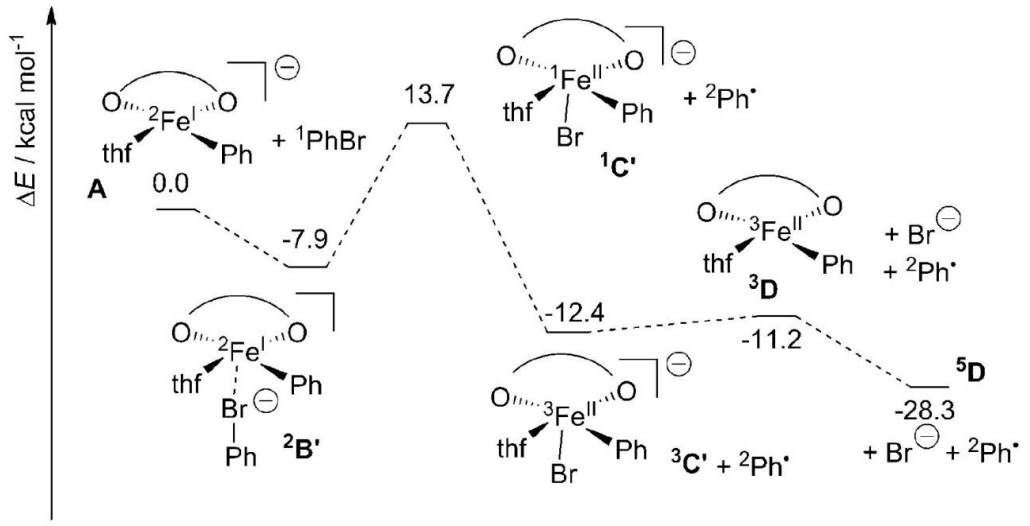


Figure 1.9. Proposed potential energy diagram for the catalytic PhBr reduction pathway.[32]

The mechanism differs from the one for iodobenzene in that species quartet $^{4}$B is now replaced by singlet species $^{1}$C. $^{1}$C happens to be the highest energy species in the profile for bromobenzene, and is the proposed explanation for the reaction not taking place in this case. The explanation is not satisfactory, as there is no analysis on why the reaction for the bromobenzene system does not go from $^{4}$B to $^{3}$C, thus avoiding the high energy intermediate $^{1}$C.

We consider the system reported by Jutand and co-workers as an interesting example of SET involving transition metals and halides. An example which is moreover related to the $Ni^{0}$ reactivity, currently subject of intense experimental research and being also under computational study in our group. We also consider that the previous computational study is insufficient, and we propose to do a more detailed analysis in this master report.

## 1.5. OBJECTIVES

Through the computational study of the reactions:

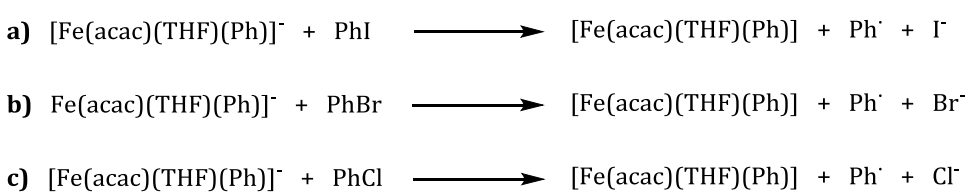


Scheme 1.1. Reactions studied in this work.

we intend to reach the following objectives:

- Clarify the reaction mechanism for the reaction between $[Fe(acac)(Ph)]^-$ and iodobenzene throught the computational characterization of key intermediates and transition states.
- Evaluate the feasibility of the mechanism for the reaction between $[Fe(acac)(Ph)]^-$ and iodobenzene for the processes involving bromobenzene and chlorobenzene and try to identify reaction trends.
- Gain a better understanding of the single electron transfer reactivity between first-row transition metals and phenyl halides and confirm the capability of density functional theory for the description of single electron transfers.

# 2. THEORETICAL ASPECTS

## 2.1. THE DFT METHODOLOGY AND THE B3LYP FUNCTIONAL[33–36]

In the first decades of the twentieth century, the theoretical basis for quantum chemistry was set. For more than 60 years, quantum chemistry focused on the multielectronic wavefunction that depends on 3N variables (where N is the number of particles of the system). An approach to this wavefunction was obtained as a solution of the time-independent Schrödinger equation. A large variety of simplifications were proposed through time, among them semiempirical, Hartree-Fock (HF) and post-HF methods. With diferent levels of computational cost and accuracy, these methods constituted for a long time the tool for most of the applications of quantum chemistry.

Density funcional theory (DFT) is an alternative approach to the wavefunction treatment described above. It started at nearly the same time as the wavefcuntion methods. Thomas and Fermi proposed in 1927 their theory of the uniform electron gas, in a six dimensional phase space (momentum and coordinates), where each electron is moving in an effective potential field that is determined by nuclear charge and assuming uniform distribution of electrons. Then, Slater theory (1951) proposed to define the exchange energy as a density functional. The final push from the theoretical side was provided by Hohenberg an Kohn, who enunciated two important theorems in 1964.[37] The first one states "the external potential $V_{ext}(\vec{r})$ is a unique functional of $\rho(\vec{r})$; since, in turn $V_{ext}(\vec{r})$ fixes $\hat{H}$ we see that the full many particle ground state is a unique functional of $\rho(\vec{r})$". This theorem demonstrates that the electron density of a system uniquely determines the Hamiltonian operator and because of it, all the properties of the system. The functional looks like:

$$E[\rho_0] = T[\rho_0] + J[\rho_0] + E_{ee,ncl}[\rho_0] + E_{Ne}[\rho_0] \qquad \text{(Eq 2.1.)}$$

where $T[\rho_0]$ is the kinetic energy (it is unknown), $J[\rho_0]$ is the classical electron-electron repulsion, $E_{ee,ncl}[\rho_0]$ is the two variables integral of the $E_{ee}$ term (it is unknown too) and , $E_{Ne}[\rho_0]$ is the nucleus-electron interaction. This is a very

important theorem because. It supposed a big forward step by reducing the number of variables from the 3N necessary in HF and post-HF methods to only 3 (x, y and z).

The second theorem states that "$F_{HK}[\rho]$ , the functional that delivers the ground state energy of the system, delivers the lowest energy if and only if the input density is the true ground state density". It represents a reformulation of the variational principle as it indicates that for a density satisfying the boundary conditions the energy obtained from the functional represents an upper bound to the exact energy $E_0$.

A year later (1965) Kohn and Sham proposed an approximation for the kinetic energy of the real system introducing the concept of a non-interacting reference system, with the same density as the real system, built from a set of orbitals such that contains the major part of the kinetic energy. This allowed to reformulate the functional expression decomposing $T[\rho_0]$ and introduced the concept of the exchange-correlation functional $E_{XC}[\rho_0]$:[38,39]

$$T[\rho_0] = T_s[\rho_0] + T_c[\rho_0] \quad \text{(Eq 2.2.)}$$

$$E_{XC}[\rho_0] = T_C[\rho_0] + E_{ee,ncl}[\rho_0] \quad \text{(Eq 2.3.)}$$

$$E[\rho_0] = T_S[\rho_0] + J[\rho_0] + E_{Ne}[\rho_0] + E_{XC}[\rho_0] \quad \text{(Eq 2.4.)}$$

Where $T_S[\rho_0]$ is the kinetic energy of non-interacting electrons. Thus, the functional can be expressed as a sum of well defined terms, with the notable exception of the last one ($E_{XC}$). This new reagrupation allowed to express the density from a set of orbitals that could be solved iteratively and giving to DFT the ability to calculate real systems.[40]

Since that point, methodological progress moved to functional development. Different treatments of the $E_{XC}[\rho_0]$ term led to diferent famílies of funcionals: the local density approximations (LDAs)[41], the semilocal generalized gradient approximations (GGAs)[42] (including the first derivative of the electronic density) and the meta-GGAs[43] (including the second derivative of the electronic density). In parallel to this methodological progress, DFT gained popularity in applied computational chemistry, and by year 2000 was already the method of choice in most cases.

The functional that will be used in this project will be a modification of B3LYP. B3LYP is a hybrid functional. By definition, hybrid functionals contain a part of HF exchange together with traditional DFT exchange. Although computationally more expensive, hybrid functionals have been demostrated to calculate interesting properties in a wide variety of systems with a reasonable quality/cost ratio.

The B3LYP functional emerged at the beginning of the nineties.[44,45] Its exchange-correlation part that unifies the Becke's three parameter exchange functional[42] and the Lee-Yang-Parr correlation functional plus 20% of exact HF exchange,[46] resulting in Eq.2.5.

$$E_{XC}^{B3LYP} = (1-a)E_X^{LSDA} + aE_x^{HF} + b\Delta E_X^B + (1-c)E_C^{LSDA} + cE_C^{LYP} \quad \text{(Eq.2.5.)}$$

a = 0.20 b = 0.72 c = 0.81

The three parameters defining B3LYP have been taken without modification from Becke's original fitting of the analogous B3PW91 functional to a set of atomization energies, ionization potentials, proton affinities, and total atomic energies.[42] Remarkably, exact exchange has proved to be important in a lot of systems, especially in those where a transition metal is used.[47–49]

## 2.2. GRIMME'S DISPERSION FUNCTION DFT-D3[50]

The DFT methods described above, which can be referred to collectively as Kohn-Sham-DFT (KS-DFT) have been very succcessful, but have their limitations. In particular, they have shown an inability to reproduce correctly the physically and chemically important London dispersion interactions. These forces are critical in highly unsaturated molecules with π-systems, or with highly electronegative atoms, but are present in practically all chemical systems. Systematic improvements to the KS-DFT methods to introduce dispersion have been studied since the first years of the XXIst century.

Grimme's DFT-D3 dispersion function is the one used in this project and has the following properties and advantages:

- It is less empirical than its predecessors. The most important parameters are computed from first principles by standard Kohn Sham Time Dependent DFT.
- The approach is asymptotically correct with all functionals for finite systems. It gives the almost exact dispersion energy for a gas of weakly interacting neutral atoms and smoothly interpolates to molecular (bulk) regions.
- It provides a consistent description of all chemically relevant elements of the periodic system (nuclear charge Z=1-94)
- Atom pair-specific dispersion coefficients and cutoff radii are explicitly computed.
- Coordination number (geometry) dependent dispersion coefficients are used that do not rely on atom connectivity information.
- It provides similar or better accuracy for "light" molecules and a strongly improved description of metallic and "heavier"systems.

Grimme's dispersion is introduced by the addition of two new terms to the classical KS-DFT formula. They are the two- and three-body energies (Equation 2.6., 2.7 and 2.8).

$$E_{DFT-D3} = E_{KS-DFT} - E_{disp} = E_{KS-DFT} - E^{(2)} + E^{(3)} \qquad \text{(Eq. 2.6.)}$$

$$E^{(2)} = \sum_{AB} \sum_{n=6,8} s_n \frac{C_n^{AB}}{r_{AB}^n} f_{d,n}(r_{AB}) \qquad \text{(Eq. 2.7.)}$$

$$E^{(3)} = \sum_{ABC} \frac{C_9^{ABC}(3cos\theta_a cos\theta_b cos\theta_c + 1)}{(r_{AB} r_{BC} r_{CA})^3} f_{d,(3)}(\bar{r}_{ABC}) \qquad \text{(Eq. 2.8.)}$$

Where C are the averaged nth-order dispersion coefficients (Eq. 2.9.), $s_n$ are scaling factors to ensure asymptotic exactness (empirical parameter) and $f$ are damping functions which determine the range of the dispersion correction (Eq. 2.10.).

$$C_9^{ABC} = \frac{3}{\pi} \int_0^\infty \alpha^A(i\omega)\alpha^B(i\omega)\alpha^C(i\omega)d\omega \qquad \text{(Eq. 2.9.)}$$

$$f_{d,n}(r) = \frac{1}{1+6\left(r/(s_{r,n}R_0)\right)^{-\alpha_n}} \qquad \text{(Eq. 2.10.)}$$

## 2.3. BROKEN SYMMETRY METHODOLOGY

Many systems in chemistry, and in particular most in organic chemistry, are closed-shell. This means that all electrons are paired; each occupied molecular orbital has one alpha and one beta electron. In terms of electron density, this means that spin density is zero at every point in space. But not all chemical systems are closed shell. Radicals for instance have one unpaired electron. This could also be treated with modifications of the standard method in most cases. In the unrestricted approach, alpha and beta orbitals are allowed to optimize independently, but they often converge to a situation where all the extra spin (usually alpha by convention) is confined to a single orbital. And each occupied beta orbital has a corresponding occupied alpha orbital. In electron density terms, this means that there is net alpha spin density in some regions of the space, but no net beta spin density at any point. In these cases, it can be said that spin symmetry is conserved. A similar situation happens when we have multiple unpaired electrons, but the system remains high spin.

There is however a more complex situation, where not all occupied orbitals are paired. This happens for systems with transition metals, radicals, highly conjugated chains... where exchange component gains importance, an unpairing of the electrons may occur giving them the possibility of electronically relax to completely different aproaches (Figure 2.1.). When this happens, the simple monodeterminantal approximation is no longer rigorously suitable.


$$\left| {}^{2}\Psi_{\text{restricted}} \right\rangle = \left| \psi_1^{(2)} \psi_2^{(1)} \right\rangle \qquad \left| {}^{2}\Psi_{\text{unrestricted}} \right\rangle = \left| \psi_3^{(1)} \overline{\psi_4^{(1)}} \psi_5^{(1)} \right\rangle$$

Figure 2.1. Left: Example of a three electron wavefunction with symmetry restrictions. Right: Example of a three electron wavefunction without symmetry restrictions.

The exact solution would be a linear combination of spin pure determinants. This cannot be done with DFT, and has to be done through multireference post-HF methods. However, this is computationally very demanding even nowadays, except for the smallest systems.

In front of this problem, an alternative proposed by Noodleman was to construct a "broken symmetry" single determinant wavefunction which does not have pure spin states,[51–53] but has monoelectronic orbitals. This cannot be expected to represent exactly the true wavefunctions of the system, as it introduces necessarily spin contamination. Nevertheless it has been proved to be able to provide quite good energies and geometries.[54] We have applied the broken-symmetry approach in this work for the calculation of systems where open-shells with alpha and beta population were present.

## 2.4. SOLVATION MODEL

The SMD[55] method is a continuum solvation model based on the description of the interaction between the quantum charge density of a solute molecule with a continuum description of the solvent. Even though this method does not use any explicit solvent molecule, it is appropriate for calculating the free energy in solution. SMD is parameterized with a few parameters such as Coulomb radii and atomic surface tension coefficients obtained from calculations and it can be used with most of the usual solvents. It is directly programmed in the Gaussian09 code for 184 solvents as water, acetonitrile, chloroform and tetrahydrofuran.

Basically, SMD computes the solvation free energy from two separate components, on one hand the bulk electrostatic contribution (treated like the most common integral-equation formalism polarizable continuum model (IEF-PCM))[56–58], and on the other hand, the cavity dispersion solvent structure term, which considers the short range interactions between the solute and solvent molecules of the first solvation shell.

## 2.5. NATURAL AND NATURAL SPIN ORBITALS

Natural Orbitals (NOs) are the unique orbitals chosen by the wavefunction itself as optimal for its own description. Mathematically, the NOs $\{\Theta_i\}$ of a wavefunction $\Psi$ can be defined as the eigenorbitals of the first-order reduced density operator $\Gamma$[14,59],

$$\Gamma\Theta_k = p_k\Theta_k \quad (k = 1,2,\dots) \qquad \text{(Eq.2.6.)}$$

In this equation, the eigenvalues $p_k$ represent the population (occupancy of the eigenfunction $\Theta_k$) for the molecular electron density operator $\Gamma$ of $\Psi$. The density operator is merely the 1-electron "projection" of the full N-electron probability distribution (given by the square of the wavefunction $|\Psi|^2$) for answering questions about 1-electron subsystems of the total wavefunction $\Psi$. Thus, $\Psi$ is the only function that enters into the definition of the NOs, and these orbitals are truly $\Psi$'s "own" (eigen) orbitals, intrinsic ("natural") to description of the electron density and other single-electron properties of $\Psi$. As for any Hermitian eigenvalues problem, the Nos form a complete orthonormal set.

Alternatively, we can characterize $\{\Theta_k\}$ as maximum occupancy orbitals. The electronic occupancy $p_\varphi$ of any normalized "trial orbital" $\varphi$ can be evaluated as the expectation value of the density operator, viz.,

$$p_\varphi = <\varphi|\Gamma|\varphi> \qquad \text{(Eq.2.7.)}$$

$$max <\varphi|\Gamma|\varphi> = p_1 \qquad (best\ \varphi\ is\ \Theta_1) \qquad \text{(Eq.2.8.)}$$

$$max <\varphi'|\Gamma|\varphi'> = p_2 \qquad (best\ \varphi' orthogonal\ to\ \Theta_1\ is\ \Theta_2) \qquad \text{(Eq.2.9.)}$$

Variational maximization of $p_\varphi$ for successive orthonormal trial orbitals leads to optimal populations $p_k$ and orbitals $\Theta_k$ that are equivalent to those in Eq.2.6., as follows from general min/max properties of eigenvalues equations. The Pauli exclusion principle insures that these occupancies satisfy $0 \le p_k \le 2$.

Natural Spin orbitals are as Natural Orbitals but generated from the spin density (with α considered positive): it is the diagonalised first-order density matrix. It appeared on the fifties.[60–62] The mathematical description of this treatment is very complex and has been described by Ugalde and co-workers in the literature.[63]

The nomenclature for Natural orbitals and for Natural spin orbitals is different. (Figure 2.1.).

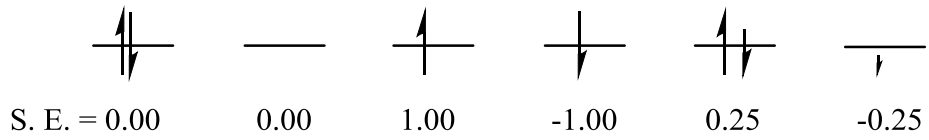


Example 2.1. Spin excess exemplification.

## 2.6. COMPUTATIONAL DETAILS

All calculations in this work were carried out with Density Functional Theory (DFT) using hybrid B3LYP-D3 functional[42,46] as implemented in Gaussian09 program.[64] A broken electron symmetry technique was used to arrive at realistic results for spin-coupled systems. All the calculations were carried out with the unrestricted version of the B3LYP functional, due to the presence of open-shell species. The D3 version of Grimme's dispersion with the original D3 damping function was added to the functional for a better system description.[50] The geometries of the reactants, transition states and intermediates were fully optimized in solution without symmetry restrictions. Vibrational frequency calculations were performed in order to characterize the stationary points as minima (without imaginary frequencies) or transition states (with one imaginary frequency). For all species, free energy corrections were applied at 298.15 K and 101325 Pa pressure including zero point energy corrections (ZPE).

In order to implement the solvation model, we selected the implicit SMD solvation methodology, where tetrahydrofuran was selected as solvent ($\varepsilon$ = 7.4257), reproducing the experimental environment.

The basis set for the calculations was LANL2TZ(f) for iron and LANL2DZdp for halides, with the corresponding effective core potentials,[65,66] and the 6-31+G* (double-$\zeta$ Pople type basis set which includes diffuse and polarization functions)[67,68] for H, C, O.

The color coding for atoms in the figures is: grey for carbon, white for hydrogen, red for oxygen, pink for Iodine, green for bromide, blue for chlorine and purple for iron.

# 3. RESULTS & DISCUSSION

## 3.1. THE CATALYST

We want to study the reactivity of the metal complex $[Fe(acac)(Ph)]^-$ with phenyl halides. The first step is the analysis of the coordination and electronic properties of the catalyst. We first considered the possibility of solvent coordination, increasing the number of bound THF molecules from 0 to 2. The resulting free energies are indicated below.

| | |
|---|---|
| $[Fe(acac)(Ph)]^-$ + 2 THF | 0.6 kcal/mol |
| $[Fe(acac)(THF)(Ph)]^-$ + 1 THF | 0.0 kcal/mol |
| $[Fe(acac)(THF)_2(Ph)]^-$ | 6.6 kcal/mol |

The most stable form happens to be with one solvent molecule attached. It has a square planar structure. This agrees with experimental suggestions. The system is experimentally known by EPR to be in a doublet state. We computed for the sake of completion the quartet states, which happens to be 10.2 kcal/ above the doublet.

The orbital analysis of the complex brings however an unexpected oxidation state on the metal. $[Fe(acac)(Ph)(THF)]^-$ has a negative charge, which leads to an initial assignment of one positive charge to Fe(I), compensated by the negative charges of two monoanionic ligands, a $\eta^2$-acetylacetonate and a phenyl. However, calculations indicate that the iron atom is actually oxidized to Fe(II). This can be seen from the analysis of natural orbitals (Figure 3.1.), spin natural orbitals (Figure 3.2.) and Mulliken spin densities (Figure 3.3.).

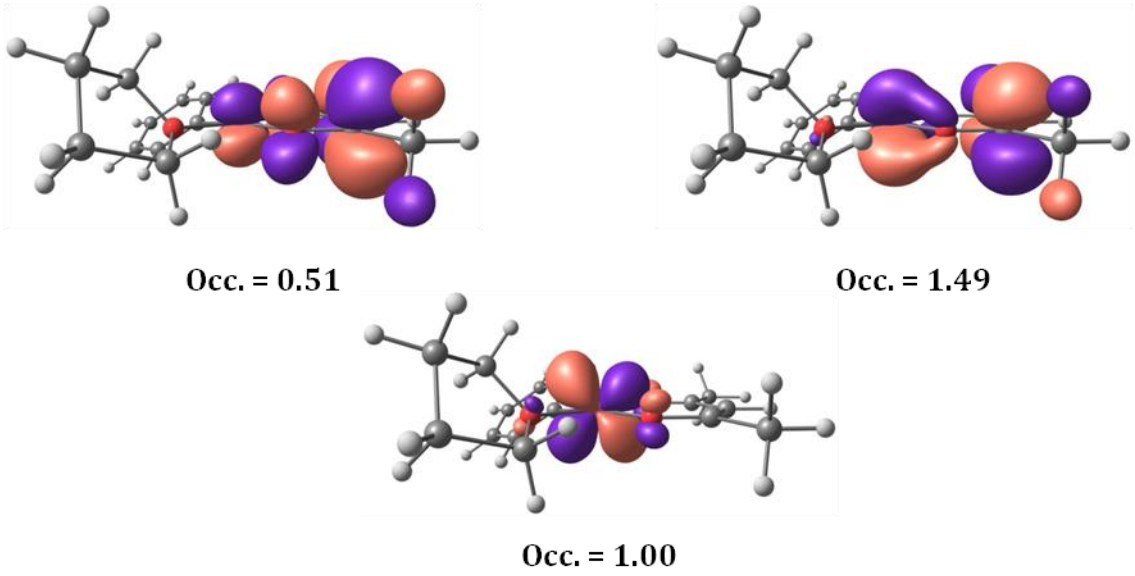


Figure 3.1. Partially filled natural orbitals for the catalyst, with indication of their occupancy.

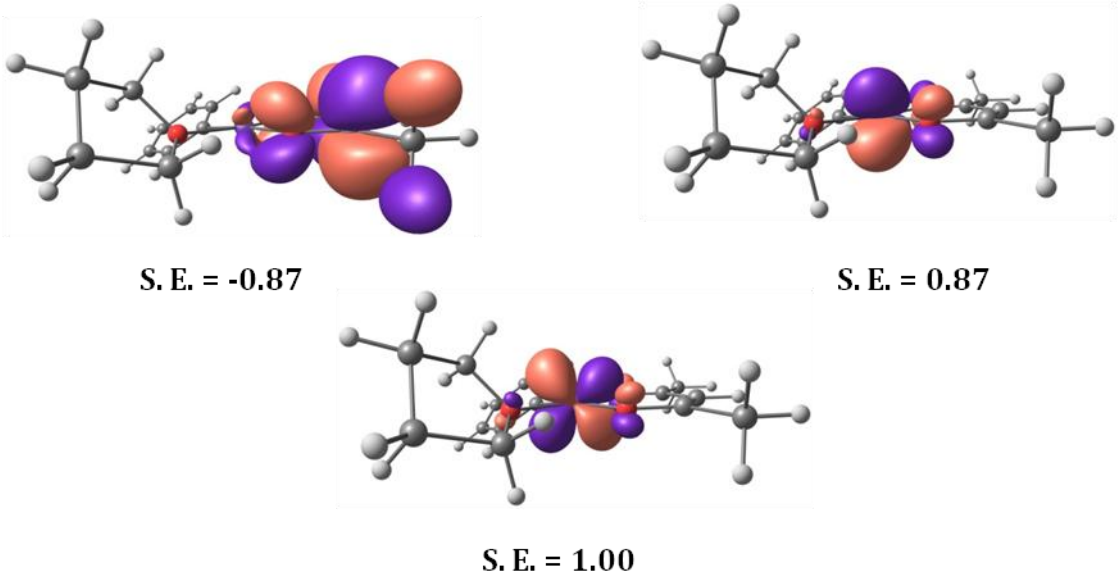


Figure 3.2. Partially filled natural spin orbitals for the catalyst, with indication of their spin excess.

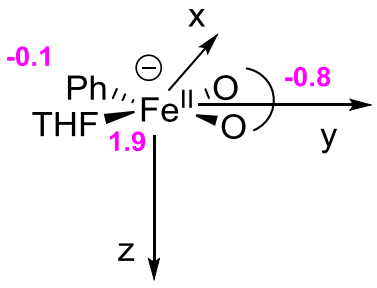


Figure 3.3. Mulliken spin densities of the catalyst.

According to Mulliken spin analysis, the acac acts as an oxidizing ligand that withdraws one electron from $Fe^{I}$ and localizes it 50% in each $C_{carbonyl}$. Ideally the electron would be completely localized in the acac and we could identify 3 single

occupied orbitals (SOMOs): two alphas centered in the iron (one in the $d_{xz}$ and the other in the $d_{yz}$) and one in the acac's π*. However, natural and natural spin orbitals shows us that $d_{xz}$ orbital possesses the same symmetry than the acac's π* so they interact originating two new orbitals but one filled with one and a half electron and the other with just half. The presence of beta density in some centers results from a symmetry broken Slater determinant. This results in spin contamination, as the $S^2$ value is 1.48 instead of the 0.75 expected for a pure doublet.

Moreover, we analyzed the acac's bond distances before coordinating and once coordinated. (Figure 3.4.)

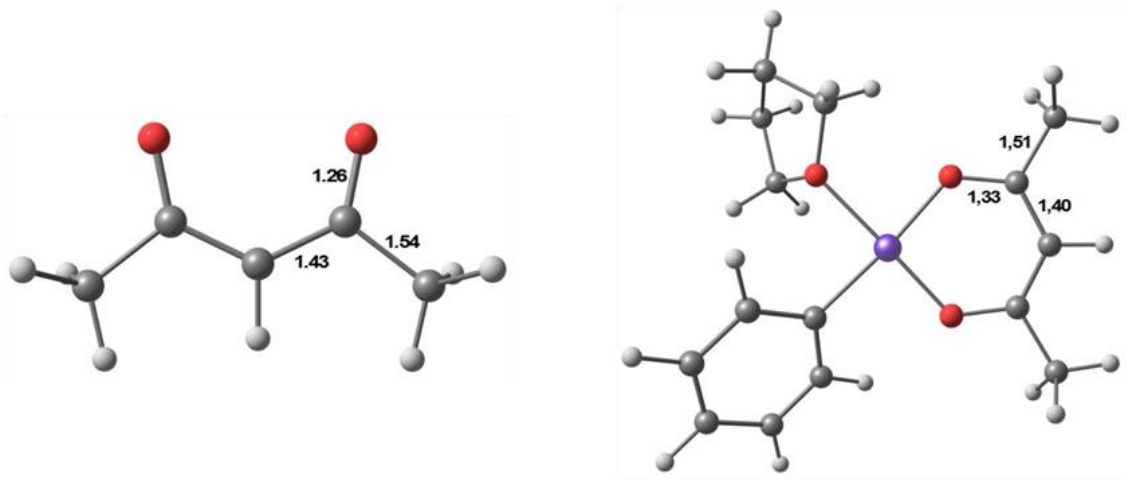


Figure 3.4. O-$C_{carbonyl}$ and $C_{carbonyl}$-$C_{\alpha}$ bond distances in free acac and catalyst.

We observe that O-$C_{carbonyl}$ bond distances have increased while both $C_{carbonyl}$-$C_{\alpha}$ bonds have reduced. That is an obvious evidence of the acac's LUMO (Figure 3.5.) being filled, since it has nodes in the carbonyl bonds but it is constructive in the α ones.

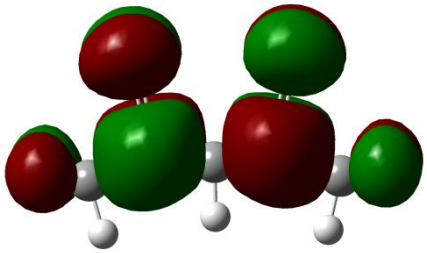

Figure 3.5. Acac's canonic LUMO.

The acac's redox properties are not so uncommon and we can find in literature cases where it acts as a reducent agent[69–71] and as an oxidant one as well as his nitrogen analogous nacnac.[72,73]

## 3.2. REACTION OF THE COMPLEX [FE(ACAC)(THF)(PH)]⁻ WITH PHI

The single electron transfer from [Fe(acac)(THF)(Ph)]⁻ to PhI (**a**) was reported in literature experimentally and computationally (Scheme 1.1.).[32]

We report in this section the calculated mechanism for reaction (**a**) (Scheme 3.2.). The free energy profile is shown in Scheme 3.2. The main steps are straightforward. Catalyst **A**, discussed in the previous section, is approached by iodobenzene resulting in adduct **B**. Electron transfer from iodobenzene to the metal moiety takes place in this adduct, resulting in intermediate **C**. Intermediate **C** can then be rearranged to intermediate **D**, which has a trigonal bypiramidal geometry, with loss of a phenyl radical. Release of the iodide anion from **D** results in the Fe(II) product **E**.

We analyze here in detail the electron transfer step from **B** to **C**. In this step, an electron is transferred from the acac reduced ligand to the C-I sigma antibonding orbital via a single electron transfer (SET) process resulting in a open-shell doublet Fe(II)-I complex plus a phenyl radical. In Scheme3.1. we can see numerically how spin density is transported from acac to Ph during the SET step. The resulting intermediate C contains an extra open shell, and its free energy in the doublet and quartet states is very similar, the latter being stable by 0.8 kcal/mol.

Remarkably, we could locate the transition state for the single electron transfer in the doublet state, and we are going to discuss the transit from **B** to **C** through **TS-B-C.**

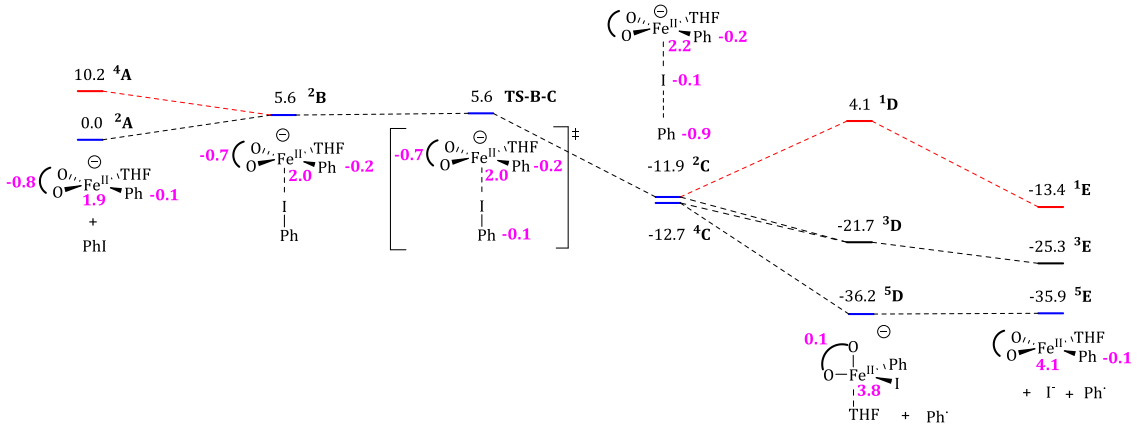


Scheme 3.1. Free energy profile (kcal/mol) for the reaction between the metal complex and iodobenzene. Mulliken spin densities in pink. Favored path highlighted in blue.

When the orbitals of intermediate **B** are analyzed, no overlap between those in iron and iodine is observed (Figure 3.7. and Figure 3.8.). This is because the iodine–iron bond is a halogen bond based in the aryl halide sigma hole: iodine possesses an electron deficiency in the extreme of the C-I bond (Figure 3.6.), that leads to a linear arrangement with the anionic metal complex. We can see that the catalyst partially occupied molecular orbitals have barely changed because of the presence of iodobenzene (Figure 3.7. and Figure 3.8.)

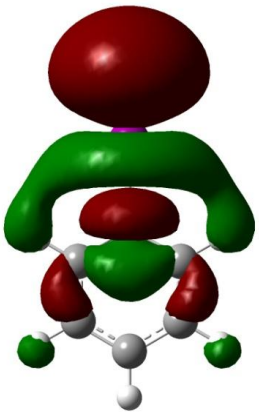

Figure 3.6. Canonic orbital corresponding to the sigma hole in iodobenzene.

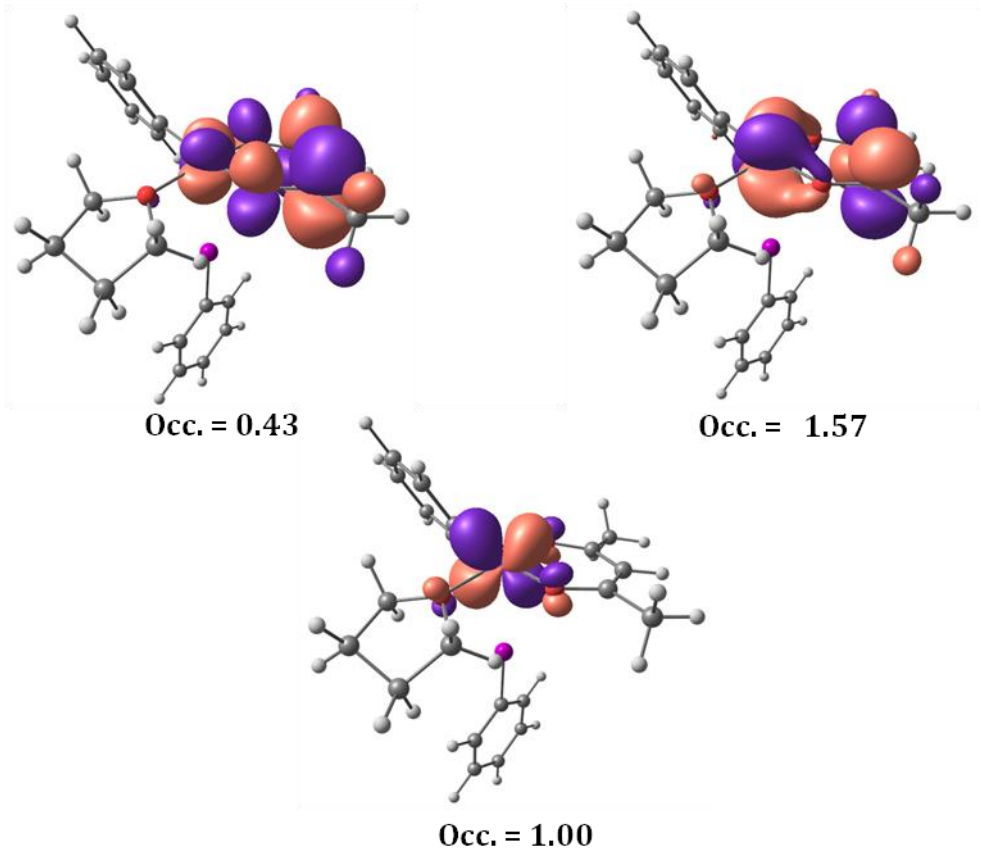


Figure 3.7. Partially filled natural orbitals for the intermediate **B**. in the reaction of iodobenzene.

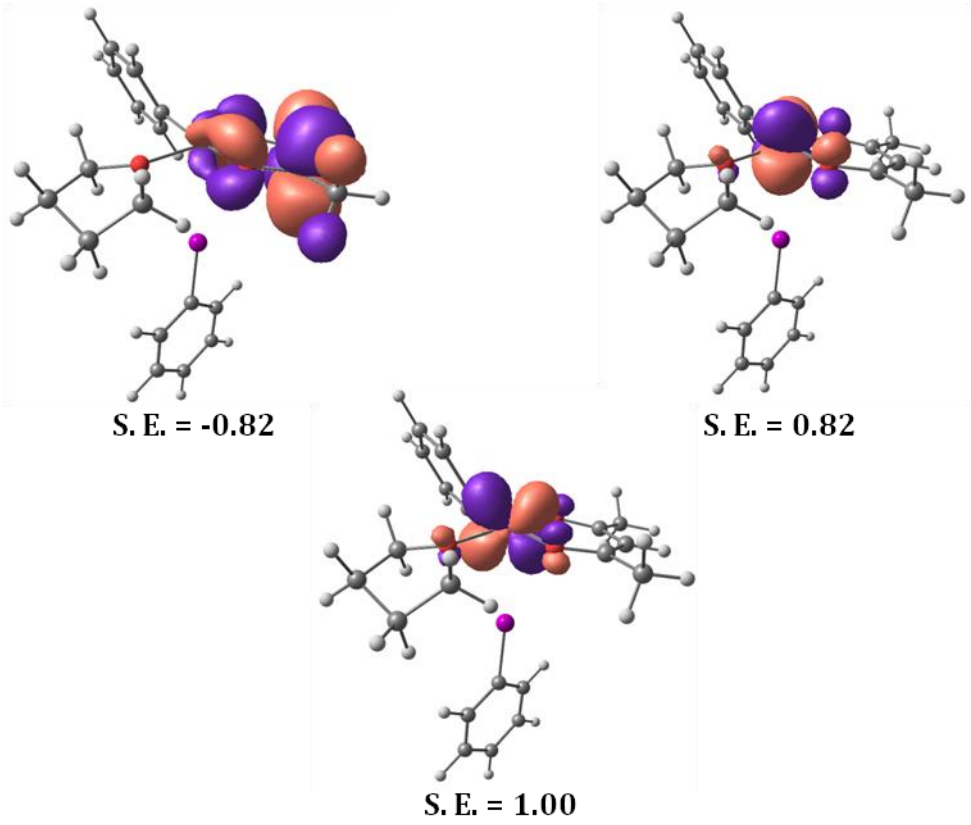


Figure 3.8. Partially filled natural spin orbitals for the intermediate **B** in the reaction of iodobenzene.

The approach of the iodine to the iron is a key trigger for the SET because orbital overlap is needed. In **TS-B-C**, the iodobenzene sigma hole interacts in the same phase with the iron doubly occupied $d_{z^2}$ orbital (Figure 3.9.). The free energy difference between **B** and **TS-B-C** is very small and consequently the TS geometry is not far from that of **B**. Some changes start to appear however on the electron distribution. The key natural and natural spin molecular orbitals of **TS-B-C** are shown in Figures 3.9 and 3.10. Some evidences of the electron transfer are already present: the acac's centered orbital is starting to lose density (the occupancy from 0.43 to 0.37 in Natural orbitals and the spin excess from -0.82 to -0.78 in Natural spin orbitals) and the partially occupied iron centered orbital accepting that electron is starting to fill (Occ. from 1.57 to 1.63 and S. E. from 0.82 to 0.78). Simultaneously, the doubly occupied $d_{z^2}$ starts to be emptied (Occ. from 1.99 to 1.98 and S. E. from 0.16 to 0.21), and the σ* C-I orbital being filled with that electron (Occ. from 0.01 to 0.02 and S. E. from -0.16 to -0.21). (Scheme 3.2). After **TS-B-C**, the process continues and intermediate **C** shows the completion of the transfer. It is an open shell doublet with two alpha electrons in the iron $d_{yz}$ and $d_{z^2}$ orbitals and one beta electron in the iodobenzene σ* orbital (Figures

3.11 and 3.12). The acac's π* orbital is now practically empty, and the irons $d_{xz}$ is almost doubly occupied.

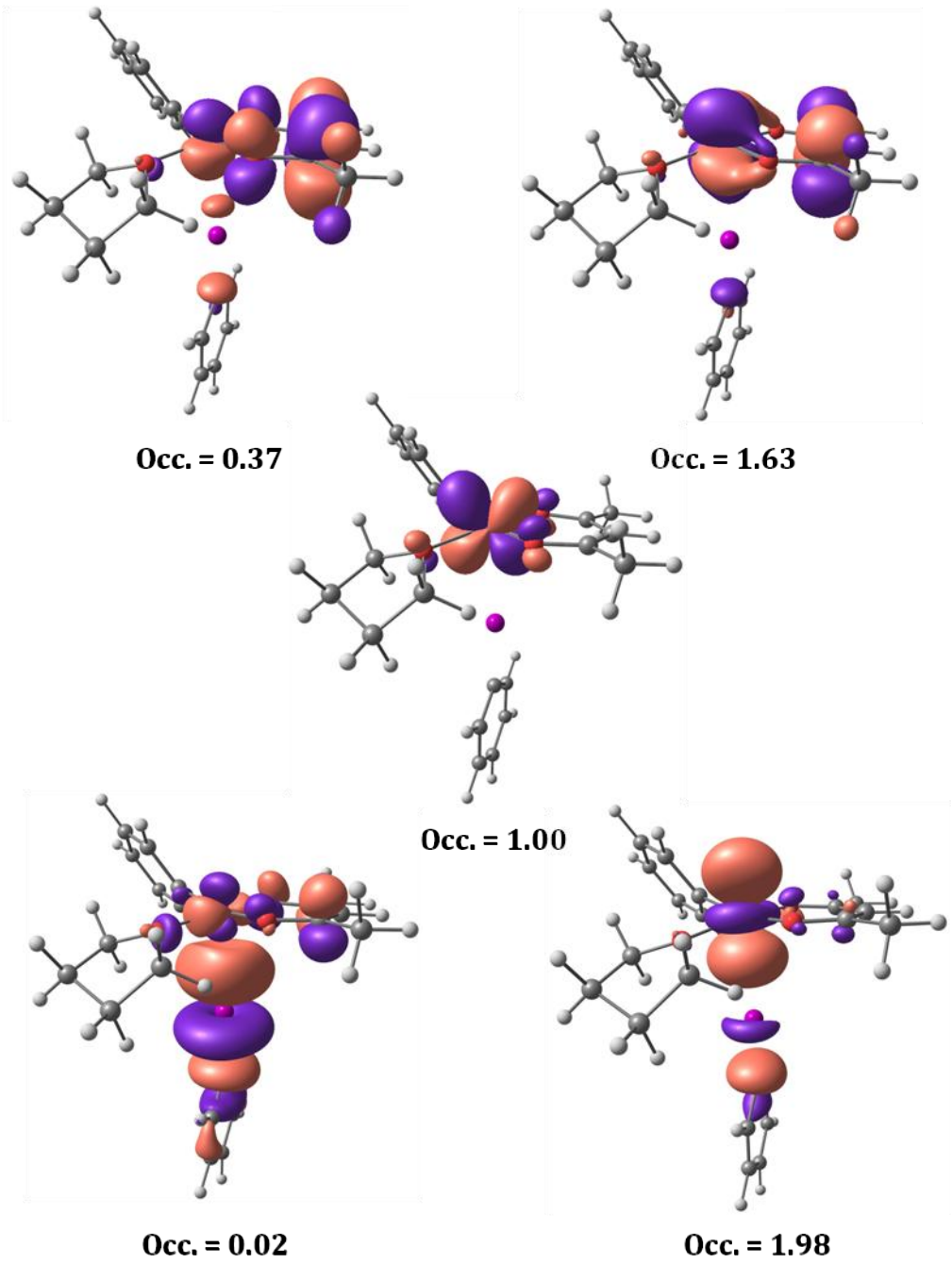


Figure 3.9. Partially filled natural orbitals for transition state **TS-B-C** in the reaction with iodobenzene.

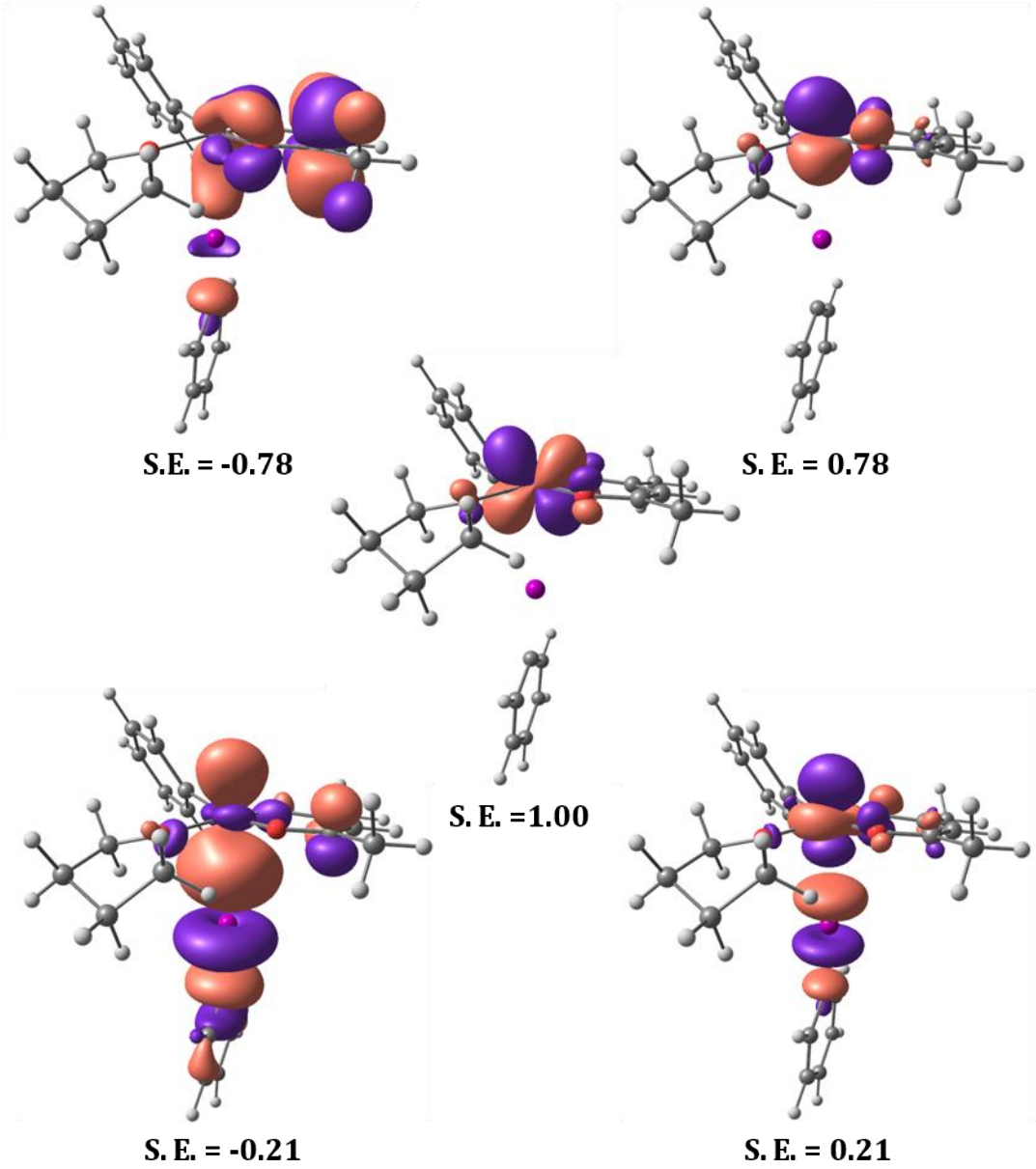


Figure 3.10. Partially filled natural spin orbitals for the transition state **TS-B-C** in the reaction with iodobenzene.

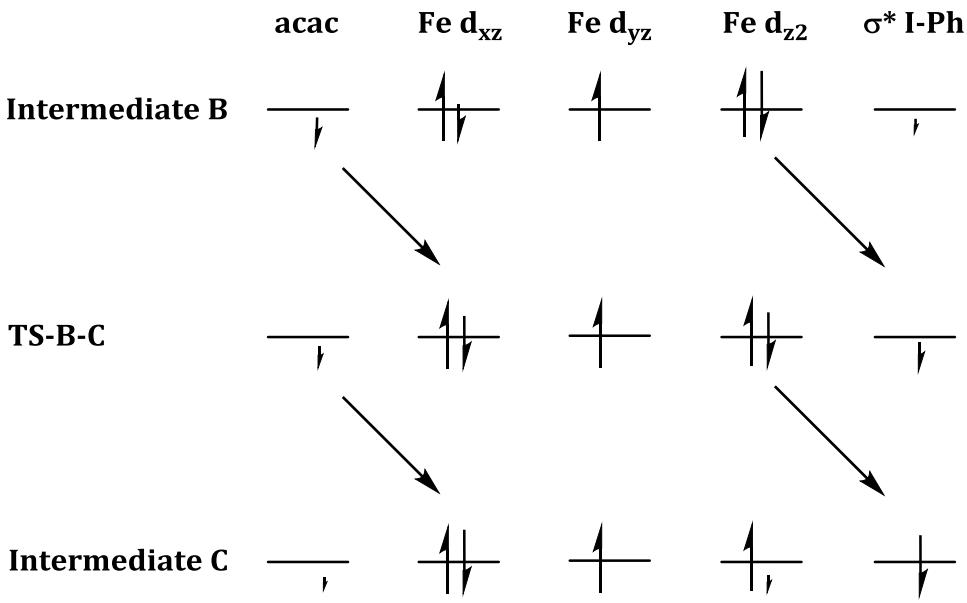


Scheme 3.2. Electron trajectories from Intermediate B to Intermediate C.

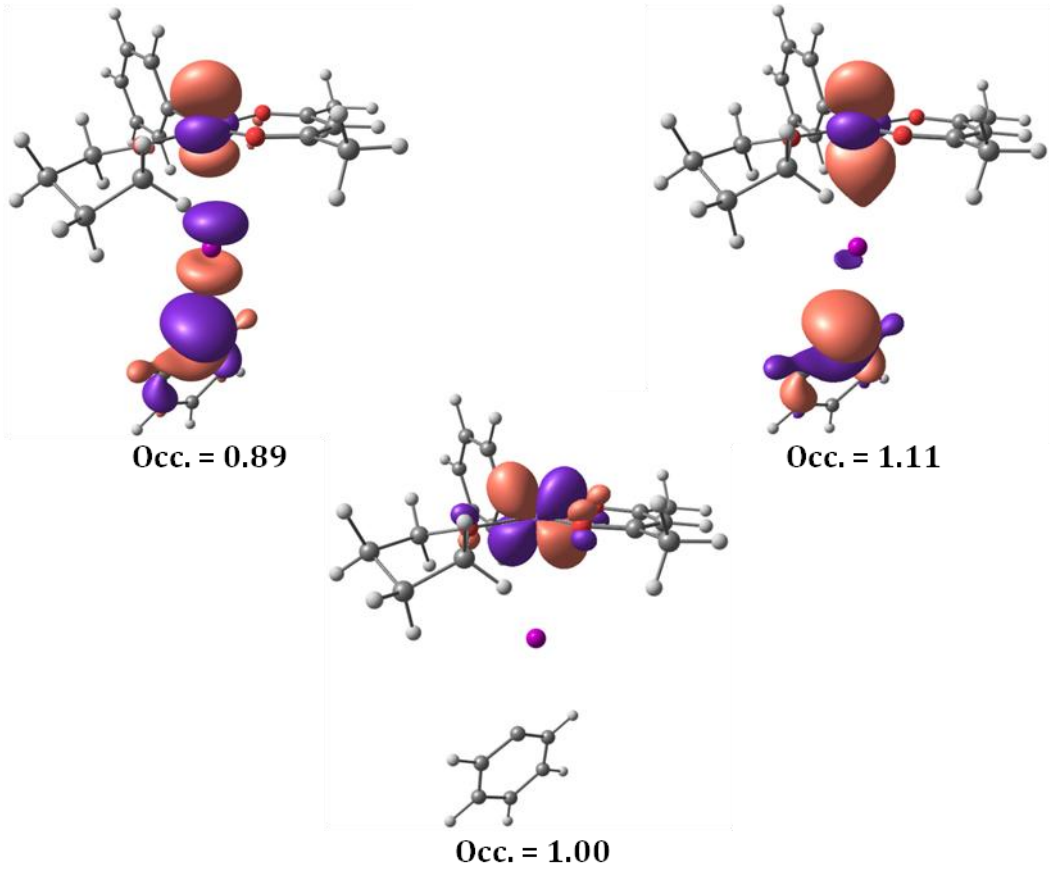


Figure 3.11. Partially filled natural orbital for intermediate **$^2$C** in the reaction with iodobenzene.

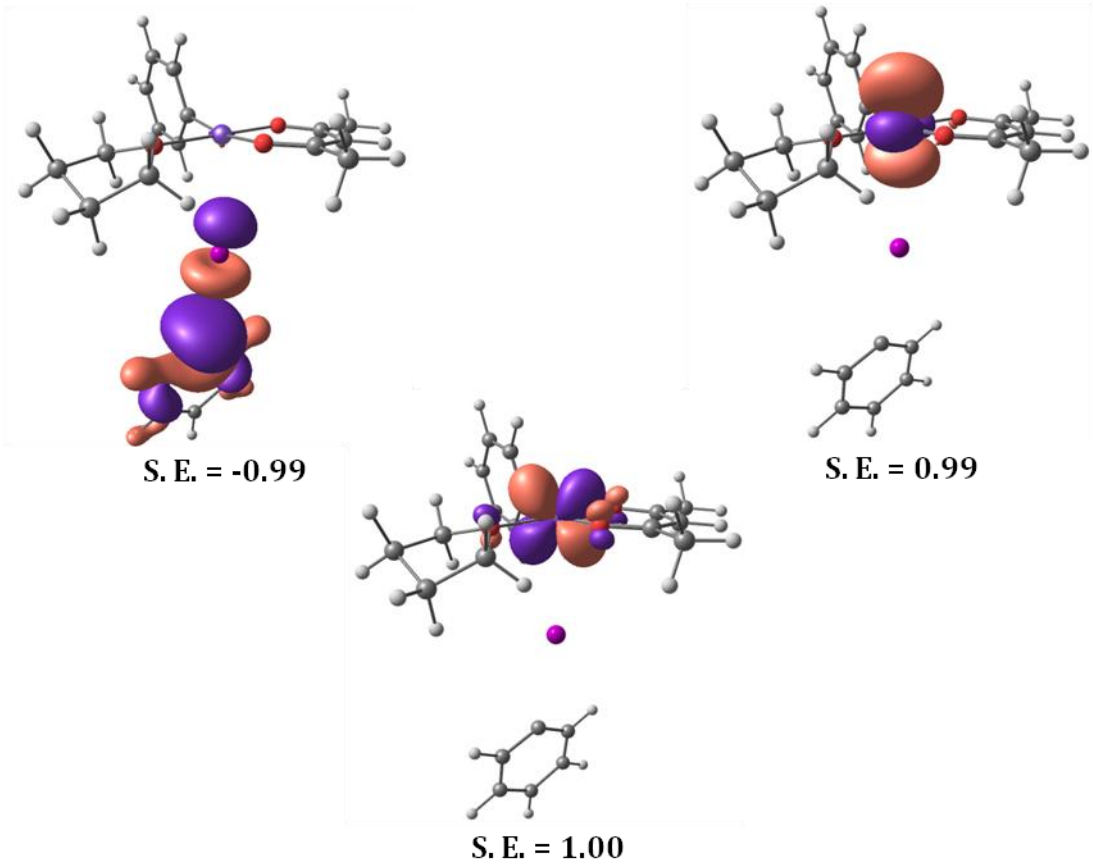


Figure 3.12. Partially filled natural spin orbitals for intermediate **$^2$C** in the reaction with iodobenzene.

Distances change all along the determining step (Figure 3.13): iodine approaches iron at first to overlap their orbitals. Simultaneously phenyl moves away from iodine since their antibonding orbitals are being filled. Next, iodine moves away from iron since there is only one partially occupied molecular orbital with constructive interaction between iodine and iron and because iron is gaining electron density.

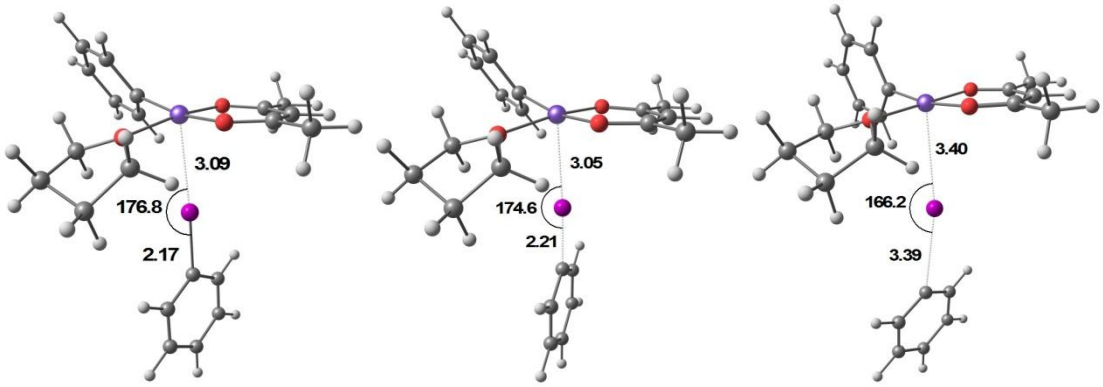


Figure 3.13. From left to right: Intermediate **B**, **TS-B-C** and Intermediate **C** for the reaction with iodobenzene**.** Ph-I···Fe key bond distances in Å and angles in degrees.

Acac's bond distances change as well (Figure 3.14) and as the reaction progresses to the unreduced acac anion, its bond distances resemble more to the free ligand (O-$C_{carbonyl}$ = 1.26 Å, $C_{carbonyl}$-$C_{\alpha}$ = 1.54 and 1.43 Å).

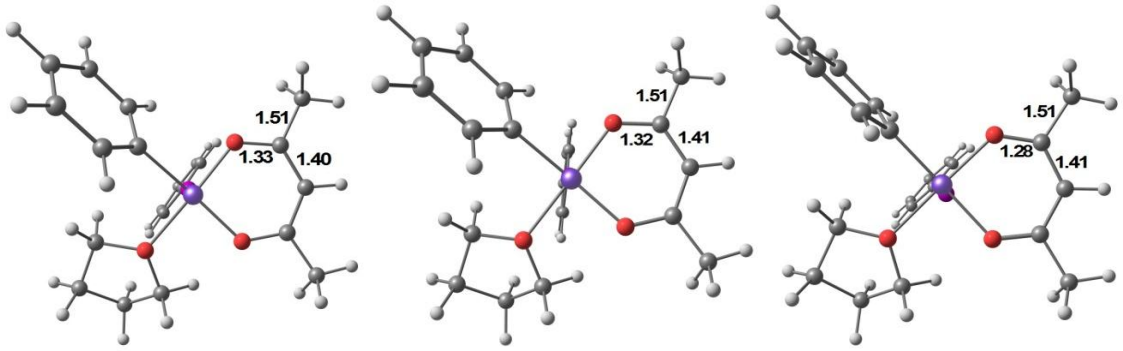


Figure 3.14. From left to right: Intermediate **B**, **TS-B-C** and Intermediate **C**. Acac's keybond distances.

The steps after **C** are not going to be discussed with so much detail, but deserve also some comment. The electronic structure of **C** is peculiar, as it contains two alpha electrons on the iron center, and a beta electron on the phenyl radical which is rather far. Because of this, the spin change in the phenyl has a minor effect, with the quartet ***$^4$C*** being only 0.8 kcal/mol below the doublet **$^2$C**. The quartet state, with two unpaired electrons on the iron center and one on the phenyl radical, is electronically similar to the doublet, but it is still suboptimal for the metal. Species **$^4$C** has an Fe(II) center with two unpaired electrons, coordination five and a square pyramidal geometry with three monoanionic ligands. The $d^6$ center has thus two doubly occupied orbital, two singly occupied and one empty In such context, one would expect a situation with four unpaired electrons on iron to be favored. This is indeed the case, the attempted calculation of **$^6$C** leads to a significant lowering of the energy. As there are also strong changes in the geometry we have labeled the resulting structure as **D**. The structure presented in the free energy profile has already removed the phenyl radical, and is thus a quintet. **D** evolves then to **E** by loss of the anion radical.

We did not compute the minimum energy crossing points (MECP) for the transition between the different multiplicity states, but they should be expected in all cases to be quite low. In any case, we provide here a characterization of the overall process, with location of all the key intermediates. The SET appears as the key step in the whole process. Its transition state has the highest energy (5.6 kcal/mol) in the overall process, and it is the key step in the chemistry of the system.

## 3.3. REACTION OF THE COMPLEX [FE(ACAC)(THF)(PH)]⁻ WITH PHBR

The path for the reaction (**b**) with bromobenzene is found to be qualitatively similar to that for the reaction (**a**) with iodobenzene (Scheme 3.3.). Coordination of the bromobenzene to the iron complex is followed by a single electron transfer from the metal complex to the phenyl bromide. After, the phenyl radical is released and the electron distribution in the metal complex is rearranged. SET is still the key kinetic step, in this case the activation barrier is higher but still affordable at room temperature, 12.5 kcal/mol.

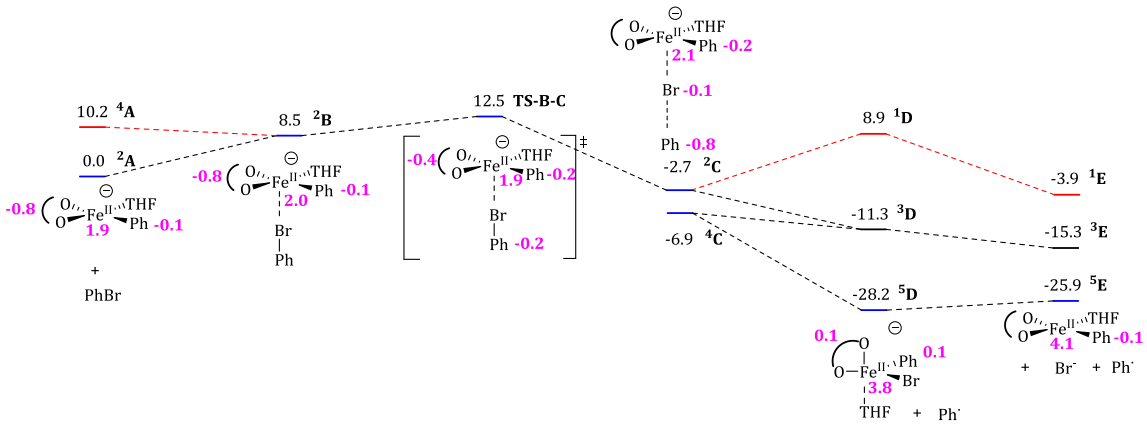


Scheme 3.3. Free energy profile (kcal/mol) for the reaction between the metal complex and bromobenzene. Mulliken spin densities in pink. Favored path highlighted in blue.

The only minor qualitative difference is the structure of intermediate ⁴C, where the Fe···X-C(Ph) is not linear, but bent (Figure 3.15.). This geometrical change is in any case likely to be associated to very minor energy differences.

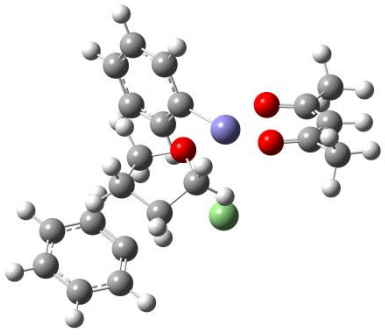

Figure 3.15. Structure of intermediate **⁴C** for the reaction with bromobenzene.

The change in electron populations in the SET from intermediates **B** to **C** is summarized in Table 3.1. The trends are analogous to those in the iodobenzene case: an electron is transferred from the acac π* orbital to the iron $d_{xz}$ orbital, and another one from the doubly occupied $d_{z^2}$ orbital to the bromobenzene's σ* orbital.

| | Natural orbitals | | | | | Natural spin orbitals | | | | |
|---|---|---|---|---|---|---|---|---|---|---|
| | **σ*** | **π*** | $d_{yz}$ | $d_{xz}$ | $d_{z^2}$ | **σ*** | **π*** | $d_{yz}$ | $d_{xz}$ | $d_{z^2}$ |
| **$^2$B** | 0.01 | 0.43 | 1 | 1.57 | 1.99 | -0.16 | -0.82 | 1 | 0.82 | 0.16 |
| **TS-B-C** | 0.02 | 0.37 | 1 | 1.63 | 1.98 | -0.21 | -0.78 | 1 | 0.78 | 0.21 |
| **$^2$C** | 0.89 | 0.00 | 1 | 2.00 | 1.11 | -0.99 | -0.07 | 1 | 0.07 | 0.99 |

Table 3.1. Occupancies of natural orbitals and spin excesses in natural spin orbitals for the SET step in the reaction with bromobenzene.

Table 3.2 collects selected geometrical parameters. The Br-C bond distance increases as the Br-C σ* orbital is filled. As bromide separates from carbon, it gets closer to the metal. The Fe-Br-C angle is slightly bent.

| | **$^2$B** | **TS-B-C** | **$^2$C** |
|---|---|---|---|
| **Fe-Br** | 3.26 | 2.90 | 2.81 |
| **Br-C** | 1.94 | 2.12 | 2.96 |
| **Fe-Br-C** | 170.4 | 167.1 | 168.5 |

Table 3.2. Fe-Br and Br-C bond distances (Å) and Fe-Br-C angles (deg) for the SET step in the reaction with bromobenzene.

Acac bond distances change again during the electron transfer as the reaction progress to the unreducted acac as we can see in Table 3.3.

| | **$^2$B** | **TS-B-C** | **$^2$C** | **Free acac** |
|---|---|---|---|---|
| **O-C$_{carbonyl}$** | 1.33 | 1.30 | 1.28 | 1.26 |
| **C$_{carbonyl}$-C$_{\alpha 1}$** | 1.51 | 1.51 | 1.51 | 1.54 |
| **C$_{carbonyl}$-C$_{\alpha 3}$** | 1.40 | 1.41 | 1.41 | 1.43 |

Table 3.3. Acac key bond distances (Å) all along the SET in the reaction with bromobenzene. Values for the free acac are also provided for comparison.

## 3.4. REACTION OF THE COMPLEX [FE(ACAC)(THF)(PH)]⁻ WITH PHCL

The mechanism for the reaction between [Fe(acac)(THF)(Ph)]⁻ and PhCl is similar to those reported above, although with a significant difference in the form of the existence of an alternative transition state for SET. The step sequence is nevertheless the same, initial adduct, key SET and release of chloride and phenyl radical coupled with electronic rearrangements in the metal complex. The computed free energy profile is presented in Scheme 3.4.

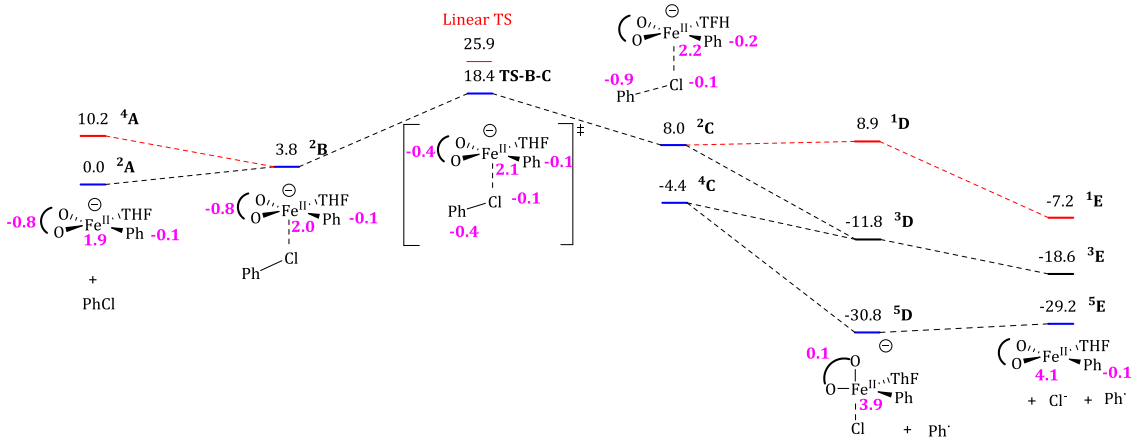


Scheme 3.4. Free energy profile (kcal/mol) for the reaction between the metal complex and chlorobenzene. Mulliken spin densities in pink. Favored path highlighted in blue.

The initial adduct B is in this case bent, with a Fe-Cl-C bond well below 180 degrees. The phenyl ring is in this case below the acac ligand. Chlorine has the smaller σ-hole of the studied halides; because of this the Fe-Cl interaction is the weakest, and the dispersion interactions between the fragments plays an important role in the formation of the adduct. We could locate two different transition states for the SET. They differ in the Fe-Cl-C angle. The linear transition state is similar to those described above for iodobenze and chlorobenzene, but its free energy of 25.9 kcal/mol is clearly higher than the 18.4 kcal/mol for the bent transition state. The bent transition state was shown through intrinsic reaction coordinate (IRC) calculations to be connected with the calculated forms of intermediates **²B** and **²C**. **²C** then evolves in a similar way to those reported above.

Both natural and natural spin orbitals were calculated but only natural spin orbitals will be discussed here. We see in Figure 3.16 that the **$^2$B** partially filled orbitals are practically the same as for the free catalyst: two alpha electrons in $d_{xy}$ and in $d_{yz}$ orbitals, respectively, and one beta electron in the acac π* orbital. The electron distribution in **TS-B-C** (Figure 3.17) is however different from those described above. Neither iron $d_{z^2}$ nor chlorine play any role in the SET: the electron transfer occurs completely by π····π interactions, between the acac full $C_{carbonyl}$ $p_z$ orbitals from the π* system, and the aromatic part of the chlorobenzene σ-hole. After the TS, the usual electron distribution is recovered in intermediate 2C, with two alpha electrons on iron and one beta electron in the phenyl (Figure 3.18).

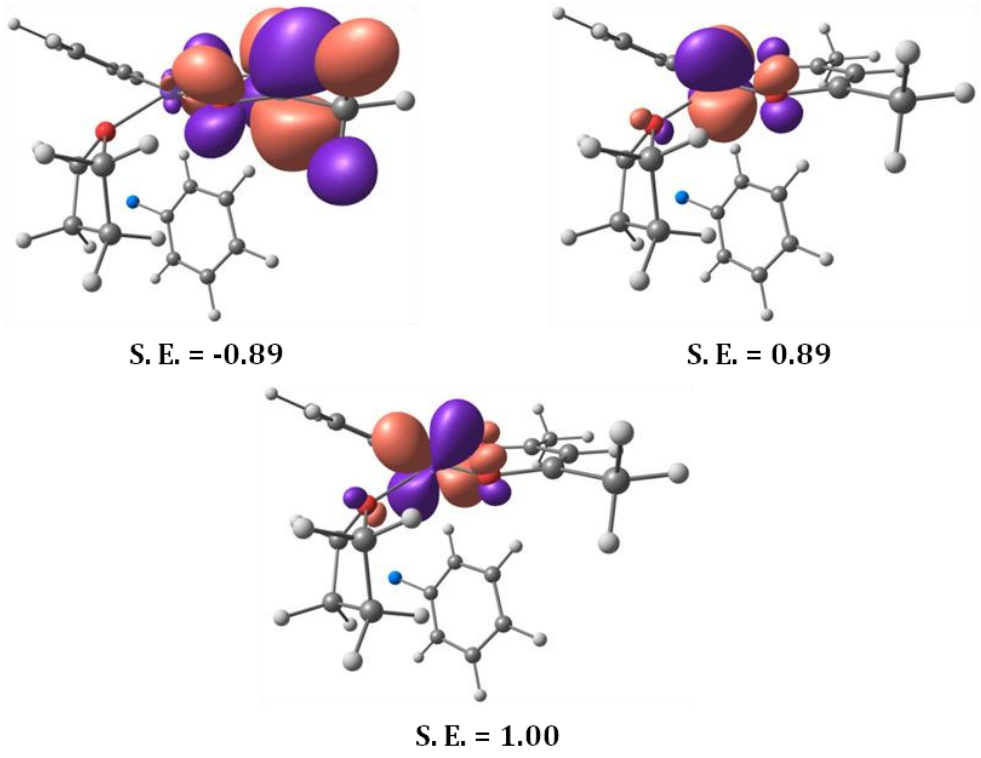


Figure 3.16. Partially filled natural spin orbitals for intermediate **B** in the reaction with chlorobenzene.

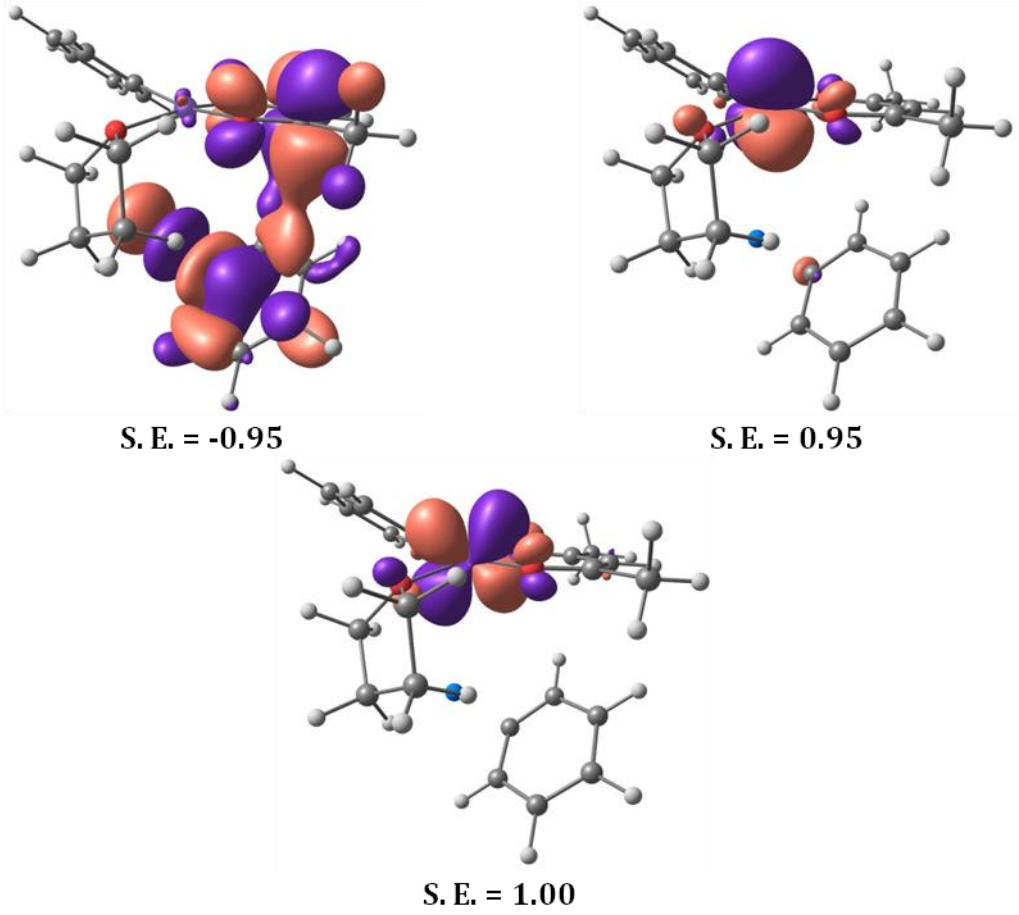


Figure 3.17. Partially filled natural spin orbitals for **TS-B-C** for the reaction with chlorobenzene.

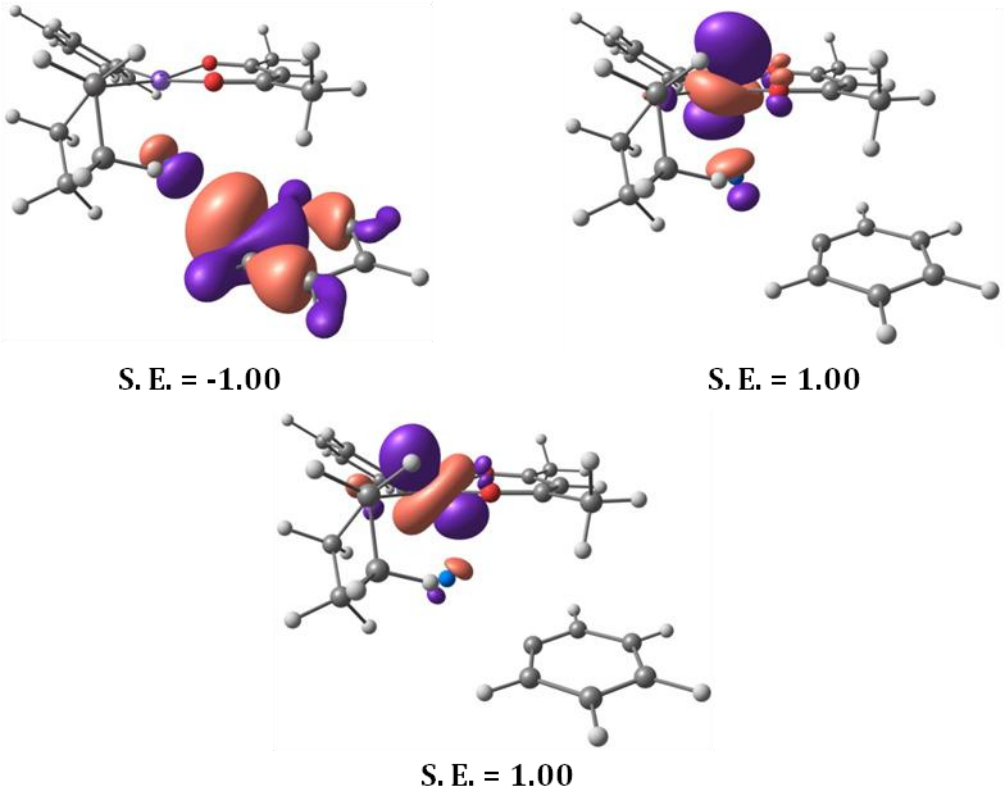


Figure 3.18. Partially filled natural spin orbitals for intermediate **$^2$C** for the reaction with chlorobenzene.

The linear TS is no longer favored for chlorobenzene because its sigma hole is so little that only weakly stabilizes a little bond angle range (Figure 1.6.) and it exhibits also a circular electron deficiency around the phenyl (Figure 3.19).

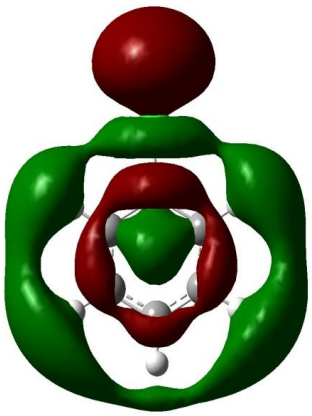

Figure 3.19. Canonical orbitals for the chlorobenzene σ-hole.

## 3.5. COMPARISON

The main difference between the studied reactions is in terms of energy barriers. Our model predicts a reduction of the energy needed to run the reaction, when increasing the atomic mass of the halogen (Table 3.4.).

| | PhI | PhBr | PhCl |
|---|---|---|---|
| **$^{2}$B** | 5.6 | 8.5 | 3.8 |
| **TS-B-C** | 5.6 | 12.5 | 18.4 |
| **$^{2}$C** | -12.7 | -6.9 | -4.4 |
| **$^{4}$C** | -11.9 | -2.7 | 8.0 |

Table 3.4. Comparision of free energies (kcal/mol) for the key intermediates for the reaction with different halobenzenes. Data for Ph-Cl correspond to the bent structures.

The responsible for these changes seems to be the carbon-halide strength: The larger the bond dissociation energy (BDE) (66.9, 82.7 and 97.3 kcal/mol for I-Ph, Br-Ph and Cl-Ph respectively),[74] the higher in energy is the LUMO and so is the energy required to fill it. This is confirmed by checking the changes in orbital occupancy and spin population along the SET step for the reactions with iodobenzene and bromobenzene (see Table 3.5.).

We observe that TS-B-C occupancies and spin excess are almost unchanged. But the π* and $d_{xz}$ orbitals are more delocalized towards the acac in PhBr than in PhI reaction. Moreover, the population of π* in $^2$B intermediate is higher in PhBr than in PhI, and the σ* of intermediate $^2$C is higher in PhI than in PhBr. We did not introduce the chlorobenzene system in this comparison because of the distorting effect of having a qualitatively different bent structure. But the fact that the linear structure has higher barriers is also conclusive.

| | PhI | | | | | PhBr | | | | |
|---|---|---|---|---|---|---|---|---|---|---|
| | **σ*** | **π*** | $d_{yz}$ | $d_{xz}$ | $d_{z^2}$ | **σ*** | **π*** | $d_{yz}$ | $d_{xz}$ | $d_{z^2}$ |
| **$^2$B** | 0.01 | 0.43 | 1 | 1.57 | 1.99 | 0.01 | 0.51 | 1 | 1.49 | 1.99 |
| **TS-B-C** | 0.02 | 0.37 | 1 | 1.63 | 1.98 | 0.02 | 0.36 | 1 | 1.64 | 1.98 |
| **$^2$C** | 0.89 | 0.00 | 1 | 2.00 | 1.11 | 0.78 | 0.00 | 1 | 2.00 | 1.22 |

| | PhI | | | | | PhBr | | | | |
|---|---|---|---|---|---|---|---|---|---|---|
| | **σ*** | **π*** | $d_{yz}$ | $d_{xz}$ | $d_{z^2}$ | **σ*** | **π*** | $d_{yz}$ | $d_{xz}$ | $d_{z^2}$ |
| **$^2$B** | -0.16 | -0.82 | 1 | 0.82 | 0.16 | -0.11 | -0.87 | 1 | 0.87 | 0.11 |
| **TS-B-C** | -0.21 | -0.78 | 1 | 0.78 | 0.21 | -0.21 | -0.77 | 1 | 0.77 | 0.21 |
| **$^2$C** | -0.99 | -0.07 | 1 | 0.07 | 0.99 | -0.98 | -0.08 | 1 | 0.08 | 0.98 |

Table 3.5. Comparision of Natural orbitals occupancies between PhI and PhBr reactions (above) and comparision of Natural spin orbitals spin excesses between PhI and PhBr reactions (down).

Thus, it is confirmed that the barrier to the SET step, and too the overall process, is strongly dependent on the nature of the halogen, and ultimately on the energy of the σ* C-X orbital. The weaker C-I bond has a lower energy σ* C-X orbital, and is thus more reactive.

# 4. CONCLUSIONS

- The mechanism for the reaction between $[Fe(acac)(Ph)]^-$ and iodobenzene resulting in [Fe(acac)(Ph)], iodide and phenyl radical, has been characterized. The starting metal complex is in fact an open shell doublet with two unpaired alpha electrons in an iron(II) center and one unpaired beta electron in a reduced acac ligand. The key step in the reaction is a single electron transfer (SET) from this complex to iodobenzene. One electron goes from acac to iron, which in turn transfers one electron to the C-I σ* orbital. We could locate the transition state for this SET, which has a broken symmetry character in DFT calculations. The free energy barrier for the process is quite low, 5.6 kcal/mol, compatible with a fast reaction at room temperature. This agrees with the experimental observation. The reaction is thermodynamically favourable with a free energy of 35.9 kcal/mol.

- The mechanism for the reaction with bromobenzene is analogous to that of iodobenzene, albeit with a slightly higher barrier 12.5 kcal/mol. For chlorobenzene, the transfer from acac to halobenzene does not happen through the metal center, but directly through space. The barrier is still feasible, with a value of 18.4 kcal/mol. Our calculations thus predict that the reaction should proceed easily with the three halobenzenes tested.

- The relative reaction rates, iodobenzene > bromobenzene > chlorobenzene follow the expected trend associated to the electronegativity of the halogen. Iodine, less electronegative, has a weaker bond to carbon, and lower lying C-I σ* orbitals, more amenable to receiving an electron transfer.

- The single determinantal DFT method is shown to perform efficiently in the description of single electron transfers, including the characterization of transition states with multiple open shells. This opens the way for a better understanding of this increasingly recognized processes in transition metal chemistry.

# 5. REFERENCES

(1) Crabtree, R. H. *New Directions in Organometallic Chemistry*; Elsevier: Switzerland, 1997.

(2) Crabtree, R. H.; Mingos, M. *Comprehensive Organometallic Chemistry III*; Elsevier: United Kingdom, 2007.

(3) Hartwig, J. F. *Organotransition metal chemistry.*; University Science Books: U.S.A., 2010.

(4) Wei, Y.; Zeng, X. *Synlett* **2015**, *27*, 650–655.

(5) Marx, V. M.; Rosebrugh, L. E.; Herbert, M. B.; Grubbs, R. H. *Top. Organomet. Chem.* **2014**, *48*, 1–17.

(6) Suzuki, A. *Angew. Chem. Int. Ed.* **2011**, *50*, 6723–6733.

(7) Jahn, U. *Top. Curr. Chem.* **2012**, *320*, 121–190.

(8) Littke, A. F.; Fu, G. C. *Angew. Chem. Int. Ed.* **2002**, *41*, 4176–4211.

(9) Smith, K. M. *Organometallics* **2005**, *24*, 778–784.

(10) Kitiachvili, K. D.; Mindiola, D. J.; Hillhouse, G. L. *J. Am. Chem. Soc.* **2004**, *126*, 10554–10555.

(11) Mindiola, D. J.; Hillhouse, G. L. *J. Am. Chem. Soc.* **2001**, *123*, 4623–4624.

(12) Basuli, F.; Bailey, B. C.; Huffman, J. C.; Mindiola, D. J. *Chem. Commun.* **2003**, *2*, 1554–1555.

(13) Basuli, F.; Bailey, B. C.; Brown, D.; Tomaszewski, J.; Huffman, J. C.; Baik, M. H.; Mindiola, D. J. *J. Am. Chem. Soc.* **2004**, *126*, 10506–10507.

(14) Theopold, K. H.; MacAdams, L. A.; Puttnual, C.; Buffone, G. P.; Rheingold, A. L. *Polym. Mater. Sci. Eng* **2002**, *86*, 310–313.

(15) Fürstner, A. *Chem. Rev.* **1999**, *99*, 991–1045.

(16) McGarrigle, E. M.; Gilheany, D. G. *Chem. Rev.* **2005**, *105*, 1563–1602.

(17) Ortiz De Montellano, P. R. *Chem. Rev.* **2010**, *110*, 932–948.

(18) Netherton, M. R.; Fu, G. C. *Palladium Org. Synth.* **2005**, *14*, 124–134.

(19) Firmansjah, L.; Fu, G. C. *J. Am. Chem. Soc.* **2007**, *129*, 11340–11341.

(20) Stille, J. K.; Lau, K. S. *Acc. Chem. Res.* **1977**, *10*, 434–442.

(21) Oturan, M. A.; Pinson, J.; Saveant, J. M.; Thiebault, A. *Tetrahedron Lett.* **1989**, *30*, 1373–1376.

(22) Andrieux, C. P.; Badoz-Lambling, J.; Combellas, C.; Lacombe, D.; Saveant, J. M.; Thiebault, A.; Zann, D. *J. Am. Chem. Soc.* **1987**, *109*, 1518–1525.

(23) Garrido-Barros, P.; Funes-Ardoiz, I.; Drouet, S.; Benet-Buchholz, J.; Maseras, F.; Llobet, A. *J. Am. Chem. Soc.* **2015**, *137*, 6758–6761.

(24) Roemelt, M.; Maganas, D.; Debeer, S.; Neese, F. *J. Chem. Phys.* **2013**, *138*, 1–22.

(25) Usharani, D.; Lacy, D. C.; Borovik, a S.; Shaik, S. *J. Am. Chem. Soc.* **2013**, *135*, 17090–17104.

(26) Argüello, J. E.; Peñéñory, A. B. *J. Org. Chem.* **2003**, *68*, 2362–2368.

(27) Li, X.-H.; Tang, Z.-X.; Zhang, X.-Z. *J. Struct. Chem.* **2009**, *50*, 34–40.

(28) Kolář, M.; Hostaš, J.; Hobza, P. *Phys. Chem. Chem. Phys.* **2015**, *17*, 23279–23280.

(29) Tamura, M.; Kochi, J. K. *J. Am. Chem. Soc.* **1971**, *93*, 1487–1489.

(30) Maximilian Czaplik, W.; Mayer, M.; Cvengroš, J.; von Wangelin, A. J. *ChemSusChem.* **2009**, *2*, 396–417.

(31) Fürstner, A.; Leitner, A. *Angew. Chem. Int. Ed.* **2002**, *41*, 609–612.

(32) Lefèvre, G.; Jutand, A. *Chem. Eur. J.* **2014**, *20*, 4796–4805.

(33) Szabo, A.; Ostlund, N. S. *Modern Quantum Chemistry*, 2nd ed.; Dover: U.S.A., 1996.

(34) Jensen, F. *Introduction to Computational Chemistry*, 5th ed.; Wiley: United Kingdom, 1999.

(35) Andrés, J.; Bertran, J. *Theoretical and Computational Chemistry: Foundations, Methods and Techniques*; Universitat Jaume I: Spain, 2007.

(36) Paniagua, J. C.; Alemany, P. *Química Quàntica*, 2nd ed.; Universitat de Barcelona: Spain, 2011.

(37) Hohenberg, P.; Kohn, W. *Phys. Rev.* **1964**, *136*, B864–B866.

(38) Kohn, W.; Sham, L. J. *Phys. Rev.* **1965**, *140*, A1133–A1138.

(39) Kohn, W.; Becke, A. D.; Parr, R. G. *J. Phys. Chem.* **1996**, *1*, 12974–12980.

(40) Kohn, W. *Rev. Mod. Phys* **1998**, *71*, 1253–1255.

(41) Jones, R. O.; Gunnarsson, O. *Rev. Mod. Phys.* **1989**, *61*, 689–746.

(42) Becke, A. D. *J. Chem. Phys.* **1993**, *98*, 5648–5652.

(43) Staroverov, V. N.; Scuseria, G. E.; Tao, J.; Perdew, J. P. *J. Chem. Phys.* **2003**, *119*,

12129–12137.

(44) Kim, K.; Jordan, K. D. *J. Phys. Chem.* **1994**, *98*, 10089–10094.

(45) Dobbs, K. D.; Dixon, D. A. *J. Phys. Chem.* **1994**, *98*, 12584–12589.

(46) Lee, C.; Yang, W.; Parr, R. G. *Phys. Rev. B* **1988**, *37*, 785–789.

(47) Reiher, M.; Salomon, O.; Hess, B. A. *Theor. Chem. Acc.* **2001**, *107*, 48–55.

(48) Holland, P. L.; Cundari, T. R.; Perez, L. L.; Eckert, N. A.; Lachicotte, R. J. *J. Am. Chem. Soc.* **2002**, *124*, 14416–14424.

(49) Yoshizawa, K.; Shiota, Y.; Yamabe, T. *J. Chem. Phys.* **1999**, *111*, 538–545.

(50) Grimme, S.; Antony, J.; Ehrlich, S.; Krieg, H. *J. Chem. Phys.* **2010**, *132*, 1–18.

(51) Noodleman, L.; Peng, C. Y.; Case, D. A.; Mouesca, J. M. *Coord. Chem. Rev.* **1995**, *144*, 199–244.

(52) Ferré, N.; Guihéry, N.; Malrieu, J.-P. *Phys. Chem. Chem. Phys.* **2015**, *17*, 14375–14382.

(53) Onofrio, N.; Mouesca, J. **2011**, *19*, 5577–5586.

(54) Blachly, P. G.; Sandala, G. M.; Giammona, D. A.; Liu, T.; Bashford, D.; McCammon, J. A.; Noodleman, L. *J. Chem. Theory Comput.* **2014**, *10*, 3871–3884.

(55) Marenich, A. V.; Cramer, C. J.; Truhlar, D. G. *J. Phys. Chem. B* **2009**, *113*, 6378–6396.

(56) Cancès, E.; Mennucci, B.; Tomasi, J. *J. Chem. Phys.* **1997**, *107*, 3032–3041.

(57) Mennucci, B.; Tomasi, J. *J. Chem. Phys.* **1997**, *106*, 5151–5158.

(58) Tomasi, J.; Mennucci, B.; Cance, E. **1999**, *464*, 211–226.

(59) Davidson, E. R. *Reduced Density Matrices in Quantum Chemistry*; Academic Press: U.S.A., 1976.

(60) Shull, H.; Löwdin, P. *J. Chem. Phys.* **1955**, *2*, 1565–1566.

(61) Löwdin, P.-O. *Phys. Rev.* **1955**, *97*, 1474–1489.

(62) Löwdin, P. O.; Shull, H. *Phys. Rev.* **1956**, *101*, 1730–1739.

(63) Piris, M.; Matxain, J. M.; Lopez, X.; Ugalde, J. M. *J. Chem. Phys.* **2009**, *131*, 1–4.

(64) Frisch, M. J.; Trucks, G. W.; Schlegel, H. B.; Scuseria, G. E.; Robb, M. A.; Cheeseman, J. R.; Scalmani, G.; Barone, V.; Mennucci, B.; Petersson, G. A.; Nakatsuji, H.; Caricato, M.; Li, X.; Hratchian, H. P.; Izmaylov, A. F.; Bloino, J.; Zheng, G.; Sonnenberg, J. L.; Hada, M.; Ehara, M.; Toyota, K.; Fukuda, R.; Hasegawa, J.; Ishida, M.; Nakajima, T.; Honda, Y.; Kitao, O.; Nakai, H.; Vreven, T.;

Montgomery, J. A.; Jr., J. E. P.; Ogliaro, F.; Bearpark, M.; Heyd, J. J.; Brothers, E.; Kudin, K. N.; Staroverov, V. N.; Kobayashi, R.; Normand, J.; Raghvachari, K.; Rendell, A.; Burant, J. C.; Lyengar, S. S.; Tomasi, J.; Cossi, M.; Rega, N.; Millam, J. M.; Klene, M.; Knox, J. E.; Cross, J. B.; Bakken, V.; Adamo, C.; Jaramillo, J.; Gomperts, R.; Stratmann, R. E.; Yazyev, O.; Austin, A. J.; Cammi, R.; Pomelli, C.; Ochterski, J. W.; Martin, R. L.; Morokuma, K.; Zakrzewski, V. G.; Voth, G. A.; Salvador, P.; Dannenberg, J. jJ.; Dapprich, S.; Daniels, A. D.; Farkas, Ö.; Foresman, J. B.; Ortiz, J. V.; Cioslowski, J.; Fox, D. J. *Gaussian 09*; 2009.

(65) Hay, P. J.; Wadt, W. R. *J. Chem. Phys.* **1985**, *82*, 270–283.

(66) Wadt, W. R.; Hay, P. J. *J. Chem. Phys.* **1985**, *82*, 284–298.

(67) Hehre, W. J.; Ditchfield, R.; Pople, J. a. *J. Chem. Phys.* **1972**, *56*, 2257–2261.

(68) Gordon, M. S. *Chem. Phys. Lett.* **1980**, *76*, 163–168.

(69) Das, A.; Kundu, T.; Mobin, S. M.; Priego, J. L.; Jiménez-Aparicio, R.; Lahiri, G. K. *Dalt. T.* **2013**, *42*, 13733–13746.

(70) Das, A.; Scherer, T. M.; Mondal, P.; Mobin, S. M.; Kaim, W.; Lahiri, G. K. *Chem. - A Eur. J.* **2012**, *18*, 14434–14443.

(71) Patra, S.; Sarkar, B.; Maji, S.; Fiedler, J.; Urbanos, F. A.; Jimenez-Aparicio, R.; Kaim, W.; Lahiri, G. K. *Chem. - A Eur. J.* **2005**, *12*, 489–498.

(72) Bart, S. C.; Lobkovsky, E.; Chirik, P. J. *J. Am. Chem. Soc.* **2004**, *126*, 13794–13807.

(73) Sylvester, K. T.; Chirik, P. J. *J. Am. Chem. Soc.* **2009**, *131*, 8772–8774.

(74) Lide, D. R. *Handbook of Chemistry and Physics*, 84th ed.; CRC Press: U.S.A., 2003.